Mon. Not. R. Astron. Soc. **322**, 43–66 (2001)

Galactosynthesis: halo histories, star formation and discs

Ari Buchalter,[1★] Raul Jimenez[2★] and Marc Kamionkowski[1★]
[1]*California Institute of Technology, Mail Code 130-33, Pasadena, CA 91125, USA*
[2]*Institute for Astronomy, University of Edinburgh, Blackford Hill, Edinburgh EH9 3HJ*

Accepted 2000 September 15. Received 2000 August 25; in original form 2000 June 12

ABSTRACT

We investigate the effects of a variety of ingredients that must enter into a realistic model for disc galaxy formation, focusing primarily on the Tully–Fisher (TF) relation and its scatter in several wavebands. In particular, we employ analytic distributions for halo formation redshifts and halo spins, empirical star formation rates and initial mass functions, realistic stellar populations, and chemical evolution of the gas. Our main findings are as follows. (a) The slope, normalization and scatter of the TF relation across various wavebands are determined largely by the parent halo properties as dictated by the initial conditions, but are also influenced by star formation in the disc. (b) TF scatter in this model is due primarily to the spread in formation redshifts. The scatter can be measurably reduced by chemical evolution, and also by the weak anticorrelation between peak height and spin. (c) Multiwavelength constraints can be important in distinguishing between models that appear to fit the TF relation in I or K. (d) Assuming passive disc evolution, successful models seem to require that the bulk of disc formation cannot occur too early ($z > 2$–3) or too late ($z < 0.2$), and are inconsistent with high values of Ω_0. (e) A simple, realistic model with the above ingredients, and fewer free parameters than typical semi-analytic models, can reasonably reproduce the observed $z = 0$ TF relation in *all* bands (B, R, I and K), as well as the observed B-band surface brightness–magnitude relation. In such a model, the near-infrared TF relation at $z = 1$ is similar to that at $z = 0$, while bluer bands show a markedly steeper TF slope at high redshift, consistent with limited current data. The remarkable agreement with observations suggests that the amount of gas that is expelled or poured into a disc galaxy may be small (though small fluctuations might serve to align B-band predictions better with observations), and that the specific angular momentum of the baryons should roughly equal that of the halo; there is little room for angular momentum transfer. In Appendix A we present analytic fits to stellar population synthesis models.

Key words: galaxies: formation – galaxies: kinematics and dynamics – galaxies: spiral – cosmology: theory.

1 INTRODUCTION

Spiral galaxies are particularly important in the study of galaxy formation, as they are believed to undergo a relatively smooth formation process, and serve as the building blocks in the formation of other galactic systems through mergers. Thus, spiral galaxies should be the easiest to model, and should provide clues as to the basic physics underlying galaxy formation. Various lines of observational evidence serve to guide our understanding of spirals, including their measured luminosity function (LF), surface brightness distribution, star formation history, chemical composition and dynamical properties. Of particular significance is the Tully–Fisher (TF) relation, a remarkably tight correlation between the luminosity and rotation speed of spirals. For a given wavelength, λ, the TF relation obeys the form

$$L_\lambda = A_\lambda V_c^{\gamma_\lambda},$$

or

$$M_\lambda = a_\lambda + b_\lambda \log V_c, \tag{1}$$

where M_λ is the absolute magnitude[1] and $b_\lambda = -2.5\gamma_\lambda$ is the slope of the relation. The debate continues as to whether this relationship results primarily from initial conditions, i.e. from the properties of the parent halo (Dalcanton, Spergel & Summers

★ E-mail: ari@tapir.caltech.edu (AB); raul@roe.ac.uk (RJ); kamion@tapir.caltech.edu (MK)

[1] An 'M' with a subscript is understood to refer to absolute magnitude in the subscripted band, while an 'M' without a subscript refers to mass.

1997; Mo, Mao & White 1998; Avila-Reese, Firmani & Hernandez 1998; Firmani & Avila-Reese 1998, 2000; Navarro & Steinmetz 2000; Mo & Mao 2000; Avila-Reese & Firmani 2000a), self-regulating feedback processes associated with star formation in the disc (Silk 1997), or a combination of both (Heavens & Jimenez 1999; Somerville & Primack 1999; van den Bosch 2000).

A TF relation arises quite naturally if one simply assumes that galactic haloes formed at roughly the same time, and that luminosity is proportional to the baryonic mass, which is in turn proportional to the halo mass. More realistically, the luminosity may depend on the galactic spin, as discs formed in high-spin haloes will be larger and of lower surface density and thus lead to lower star formation rates. Still, even with spin, a TF relation arises if haloes all formed at roughly the same epoch. In both cases (with and without spin), scatter in the redshift of halo formation should lead to scatter in the central densities of the haloes and thus to scatter in the TF relation.

Several groups have made considerable progress in understanding spiral-galaxy properties along these lines using semi-analytic models (SAMs). Eisenstein & Loeb (1996, hereafter EL96) used Monte Carlo realizations of halo formation histories to calculate the minimum TF scatter that should arise from the spread in halo formation times. They concluded that, unless spirals form at $z \gtrsim 1$, without subsequently accreting much mass, the TF relation cannot arise simply from initial conditions, but must instead be due to some feedback mechanism that decouples the luminosity from the halo history.

More recently, other groups have investigated detailed SAMs of disc-galaxy formation which incorporate such features as formation histories derived directly from *N*-body simulations, universal halo profiles, adiabatic disc contraction, bulge formation via stability criteria, star formation, supernova feedback, dust, cooling and mergers (Firmani & Avila-Reese 1998, 2000; Somerville & Primack 1999; van den Bosch 2000; Navarro & Steinmetz 2000). Their conclusions differ as to the relative importance of initial conditions versus feedback from star formation and/or supernovae in defining the TF relation. These studies generally agree, however, that the spread in halo formation redshifts is a significant source of scatter in the TF relation, and that reconciling models with TF observations seems to require a low matter density ($\Omega_0 \sim 0.3$–0.5) and disc formation at high redshift ($z \gtrsim 1$).

One powerful test of such models, which has not been fully appreciated, is the simultaneous comparison of their predictions to TF data from *several* wavebands. Some previous work has considered only an assumed value for the mass-to-light ratio in a given band, rather than using stellar population models to predict broad-band magnitudes, and many authors have investigated TF predictions for only a single waveband, typically *I* or *K*, where the observed TF scatter is the smallest [$\sim$0.4 mag in the most carefully defined samples (Willick et al. 1995, 1996, 1997; Tully et al. 1998)]. Since these wavelengths measure primarily the oldest, shell-burning, stellar populations, such measurements are, by construction, sensitive only to the total luminous mass of the galaxy and to little else. Thus, while some authors have claimed success in fitting the near-infrared (near-IR) TF relation, their predictions in bluer bands, where many model ingredients would be most strongly manifested owing to the younger populations probed, have gone unchecked. With realistic stellar population models, the leverage gained by spanning a range of wavelengths should therefore be crucial in distinguishing models that produce similar near-IR TF predictions and help to assess the importance of various SAM features. Heavens & Jimenez (1999, hereafter HJ99) used a simple halo and disc model combined with empirical star formation properties to investigate the role of star formation in the TF relation, examined the simultaneous constraints from various wavebands, but did not address some of the other key considerations listed above.

Our approach here will focus on constructing, as much as possible, a model 'from the ground up', i.e. starting with a minimal set of simple, well-motivated assumptions and individually investigating the impact of various plausible modifications. In essence, we are asking whether a plausible model with fewer free parameters[2] than are usually incorporated into current SAMs can reasonably pass various observational tests. Though the resulting model will lack many of the sophisticated features of other SAMs and will surely be an oversimplification in many respects, it may shed important light on the issue of which physical ingredients are truly essential in determining certain disc properties.

We build on the work of HJ99, using their halo/disc model and stellar populations code, but generalizing it to include a variety of important features, such as analytic models for the distribution of halo formation redshifts and spins (as well as the predicted anticorrelation between the two). This allows us to assess not only the impact of these distributions on TF predictions, but the dependence on cosmological parameters and the power spectrum as well. We also include for the first time an analytic description of chemical evolution. This measurably reduces the scatter in the TF relation, which is found to arise mainly from the spread in formation times. The overall result will be a model for disc galaxies that can reproduce the observed TF relation, locally and at $z = 1$, in all relevant wavebands *with the right magnitude of scatter*, and roughly fit the observed surface brightness distribution of spirals. The model necessitates cosmological parameter values that are in line with current estimates, and requires that the bulk of disc formation occurs in the range $0.4 < z < 2$, with little activity at the present day or beyond $z \sim 3$. This agreement implies that, although plausible, other mechanisms that would add or remove gas from the disc (such as mergers, gas expulsion by supernovae, etc.), and thereby distort the predicted luminosity, are not necessarily required to predict successfully these global disc-galaxy properties.

2 THE MODEL

2.1 Our starting point

We build on the skeletal disc-galaxy model of HJ99. We review the basic ingredients here and refer the reader to HJ99 for a more complete description. This model assumes that, after dark haloes separate from the Hubble flow and collapse, they subsequently relax to an isothermal sphere of mass M, and the baryons instantaneously settle into a central disc with mass[3] $M_{\rm d} = m_{\rm d} M$, where $m_{\rm d} = \Omega_{\rm b}/\Omega_0$, Ω_0 is the present-day non-relativistic matter density in units of the critical density, and the baryon density, $\Omega_{\rm b}$, is set by nucleosynthesis, $\Omega_{\rm b} = 0.019\,h^{-2}$ (Tytler et al. 1999). The disc is assumed to have an exponential

[2] Most of the freedom in our models comes from the cosmological parameter choices, which we generally fix to be consistent with current estimates; other choices for these parameters would yield other TF relations, usually inconsistent with the data.

[3] Other workers have shown that TF results are fairly insensitive to the precise value of the assumed disc mass fraction (Firmani & Avila-Reese 2000).

profile, $\Sigma(R) = \Sigma_0 \exp(-R/R_d)$, with central surface density Σ_0 and scalelength R_d, such that $M_d = 2\pi\Sigma_0 R_d^2$. Since the assumptions of a singular isothermal sphere and instantaneous disc formation cannot strictly be true, the apparent success of the model suggests that details such as the profile shape (Mo & Mao 2000) or disc contraction process may not be of primary importance in determining the resultant global properties of spirals.

With the gaseous disc in place at the time of formation, star formation proceeds according to an empirical Schmidt law, such that the star formation rate (SFR) depends only on the local gas surface density, Σ_g, via the empirical relation $\Phi_{SFR} = B\Sigma_g^{1.4}$ where $B = 9.5 \times 10^{-17}$ in SI units (Kennicutt 1998). Given the conservation of baryonic mass, the total SFR, as well as remaining gas fraction, can then be obtained as functions of time since formation, t, by integrating over the disc, yielding respectively

$$\dot{M}_*(t) = \frac{50\pi B R_d^2 \Sigma_0^{1.4}}{49}\, {}_3F_2(3.5, 3.5, 3.5; 4.5, 4.5; -a), \tag{2}$$

$$\dot{M}_g(t) = 2\pi R_d^2 \Sigma_0\, {}_3F_2(2.5, 2.5, 2.5; 3.5, 3.5; -a), \tag{3}$$

$$a = 1.06[H(z)]^{0.4} \left(\frac{t}{\mathrm{Gyr}}\right) \left(\frac{V_c}{250\,\mathrm{km\,s^{-1}}}\right)^{0.4} \left(\frac{\lambda}{0.05}\right)^{-0.8} \left(\frac{m_d}{0.05}\right)^{0.4}, \tag{4}$$

where λ is the spin parameter[4] and $H(z)$ is defined in equation (6) [see equations (3)–(9) in HJ99]. The model ignores any gas returned to the interstellar medium (ISM) by stars as well as late infall of fresh gas.

Using the SFR and an assumed stellar initial mass function (IMF), the properties of the stellar populations formed at each time interval are calculated using the spectrophotometric stellar evolution code of Jimenez et al. (1998, 2000), and broad-band magnitudes derived from the resulting spectra are integrated over the life of the galaxy to yield luminosities in various bands (see Appendix A). Other stellar population codes generally yield results that agree to within 0.1–0.2 mag and have comparable dispersions (Jimenez et al. 2000). Since we are integrating the SFR over time, weighted by the specific luminosities of model stellar populations as a function of age, metallicity, spin, etc., the model can predict disc luminosities and surface brightnesses (in a variety of wavebands) at any point in their evolution. More details about the calculation of the luminosities of the stellar populations, as well as some possibly useful analytic fitting formulae, are provided in Appendix A.

To summarize, for a given set of cosmological parameters, the model of HJ99 takes as input a total galactic mass, M, and spin parameter, λ, and can output, as functions of time, the disc luminosity and surface brightness in various wavebands, as well as the metallicity.

2.2 Spherical collapse model

Our model will of course depend on the background cosmogony, which effectively sets the initial conditions and dictates the course of structure formation. We consider various cold dark matter (CDM) models with a power spectrum given by $P(k, z) = AD^2(z)k^nT^2(k)$, where A is the overall amplitude, $D(z)$ is the linear growth factor and k^n is the primordial power spectrum (we shall assume an untilted, $n = 1$ primordial spectrum throughout). For the transfer function, $T(k)$, we adopt the functional form of Bardeen et al. (1986), parametrized by the shape parameter Γ. We restrict our study to flat geometries ($\Omega_0 + \Omega_\Lambda = 1$, where Ω_Λ is the energy density associated with the cosmological constant, in units of the critical density) and consider various values of h, the Hubble parameter (H_0) in units of $100\,\mathrm{km\,s^{-1}\,Mpc^{-1}}$.

We will be interested in the relation between the size and mass of a galactic halo, and this is fixed by the formation redshift – haloes of a given mass that undergo collapse earlier are expected to be smaller and denser – through the spherical collapse model. Since we adopt an isothermal profile, we follow HJ99 and take the radius of the halo to be the value at which the enclosed mass density is 200 times the critical density at the redshift of formation (see Mo, Mao & White 1998). We thus have

$$V_c = [10GMH(z)]^{1/3}, \tag{5}$$

where

$$H(z) = H_0[\Omega_0(1+z)^3 + (1 - \Omega_0 - \Omega_\Lambda)(1+z)^2 + \Omega_\Lambda]^{1/2} \tag{6}$$

and V_c is the circular velocity required for centrifugal support in the potential of the halo.

The Press–Schechter (PS) theory will be our starting point for calculating halo abundances and formation times. The theory states the familiar result that the comoving number density of haloes in a mass interval dM about M at redshift z is given by

$$n(M, z)\,\mathrm{d}M = -\sqrt{\frac{2}{\pi}} \frac{\rho_b}{M} \frac{\delta_c}{\sigma^2(R, z)} \frac{\mathrm{d}\sigma(R, z)}{\mathrm{d}M} \exp\left[-\frac{\delta_c^2}{2\sigma^2(R, z)}\right] \mathrm{d}M, \tag{7}$$

where $R^3 = 3M/4\pi\rho_b$, ρ_b is the constant, comoving background matter density, $\sigma(R, z)$ is the rms fractional density perturbation in spheres of radius R, and δ_c is the linear overdensity at collapse, which is here understood to depend on redshift via an empirically derived relation (L. Wang, private communication). The limitations of the PS formalism are discussed in Section 4.

It should be noted that, while accurate in the Einstein–de Sitter (EdS) case, equation (5) is not a precisely correct mapping of M to V_c for arbitrary cosmogonies, since it is the ratio of the halo density to the *background* density [which varies with redshift differently from $H(z)$], not the critical density, which sets the stage for collapse. Furthermore, the choice of 200 for the value of this ratio is appropriate for the spherical collapse model in an EdS universe, but it can vary substantially from this value for other cosmological models. Wang & Steinhardt (1998) follow a more detailed approach to calculate precisely the virial relation for a universe with arbitrary vacuum energy density. This approach, however, requires the calculation of the halo potential energy. Since, for analytic simplicity, we have adopted a singular isothermal sphere profile, the potential energy is formally infinite. One remedy would be to use truncated profiles. Applying the formalism of Wang & Steinhardt (1998), we investigated a suite of truncated models with various density profiles and found that, within a constant factor of order unity, equation (5) is an excellent approximation to the analytic results in these cases, with the small discrepancies vanishing towards higher redshifts where any cosmogony approaches an EdS model. Given these negligible differences, we retain the singular isothermal model and employ equation (5) above in the spirit of simplicity that underlies our present approach.

Ultimately, this ambiguity in the M–V_c mapping translates only

[4] The symbol 'λ' is understood to refer to spin parameter, except when appearing as a subscript, in which case it refers to waveband.

into an uncertainty in the normalization of V_c and thus to a possible uncertainty in the absolute values of some of our model predictions; relative differences between models are largely unaffected.[5] It will be shown, however, that our predictions for the TF relation and surface brightness–magnitude relation are in practice highly insensitive to this uncertainty, since it will impact both axes of these relations with generally little or no net effect, as shown in Section 4.

2.3 Formation redshift distribution

In standard hierarchical models of structure formation, haloes of a fixed mass form over a range of redshifts. HJ99 examined only fixed values for the redshift of formation, z_f, for haloes, but considered several values to illustrate the effect of a spread in z_f. EL96 performed Monte Carlo realizations of halo formation histories, using the merger-tree approach (Lacey & Cole 1993, 1994) and a spherical accretion model, and concluded that the minimum TF scatter resulting solely from the calculated spread in halo formation redshifts is already uncomfortably larger than that observed. They concluded that satisfying the upper limit of a $\sim$10 per cent relative error in velocity dispersion requires that $\Delta z_f/(1+z_f) \lesssim 20$ per cent. Other workers (e.g. van den Bosch 2000) have looked at the scatter in formation redshifts (or the closely related scatter in 'concentration parameters') obtained from numerical simulations and found better agreement with the observed scatter.

Although numerical simulations should in principle provide the best way to evaluate the formation redshift distribution, these have limitations in practice. In particular, it is difficult to collect enough statistics to determine the distributions for different masses and/or to determine how these distributions depend on the cosmological parameters or the power spectrum. As the analytic distributions discussed below demonstrate, it *is* indeed to be expected that the formation redshift distribution (and thus resulting scatter in the TF relation) should depend on the mass, cosmological parameters and power spectrum. Thus, although they can provide some order-of-magnitude estimates, results from numerical simulations can be misapplied in SAMs if they are determined, say, for one mass from a simulation with a particular choice of cosmogony and then applied to other masses and/or cosmogonies. Moreover, analytic methods allow for more obvious and direct insight into the dependence of the model on various parameter choices and assumptions.

Therefore, we follow Viana & Liddle (1996) and explore two plausible analytic models for the distribution of halo formation redshifts. The first, denoted as the 'S' distribution, is that of Sasaki (1994), which simply uses the PS formalism to calculate the formation rate of bound objects, weighted by the probability of arriving at some later time without merging, under the assumption that the destruction efficiency is independent of mass. In this model, the distribution of formation redshifts of haloes with mass M is given by

$$\frac{\mathrm{d}n_S}{\mathrm{d}z_f} = -\frac{\delta_c^2}{\sigma^2(R,z_f)}\frac{n(M,z_f)}{\sigma(R,0)}\frac{\mathrm{d}\sigma(R,z_f)}{\mathrm{d}z_f}. \quad (8)$$

The S distribution has the advantage of being independent of how one defines a new halo, but the assumption of self-similar merging might be questioned (see, e.g., Percival, Miller & Peacock 2000).

[5] We thank the anonymous referee for focusing our attention on this issue and for providing useful and valuable suggestions.

The second distribution, denoted as the 'LC' distribution, addressed this shortcoming by employing the merger-tree approach of Lacey & Cole (1993, 1994). In this formalism, haloes continually grow with time, and so one must explicitly define the time at which a particular halo has come into existence[6] (e.g., the epoch at which the largest progenitor has half the present-day halo mass). Lacey & Cole (1993) derived expressions for the expected z_f distribution of haloes using both analytic counting arguments and a Monte Carlo approach to generate merger histories for $M(t)$ explicitly. They found that the former approach yielded excellent agreement with N-body results, while the latter overestimated halo ages (Lacey & Cole 1994). Their results did not depend strongly on the value of the local slope of the power spectrum. The z_f distribution in this model is given by

$$\frac{\mathrm{d}n_{LC}}{\mathrm{d}z_f} = p(w(z_f))\frac{\mathrm{d}w(z_f)}{\mathrm{d}z_f}, \quad (9)$$

where

$$p(w(z_f)) = 2w(z_f)(f^{-1}-1)\,\mathrm{erfc}\left(\frac{w(z_f)}{\sqrt{2}}\right) - \sqrt{\frac{2}{\pi}}(f^{-1}-2)\exp\left[-\frac{w^2(z_f)}{2}\right], \quad (10)$$

$$w(z_f) = \frac{\delta_c[\sigma(M,0)/\sigma(M,z_f)-1]}{\sqrt{\sigma^2(fM,0)-\sigma^2(M,0)}}, \quad (11)$$

and f is the fraction of halo mass assembled by formation redshift z_f. Thus at fixed redshift, models with higher values of f produce younger galaxies. Lacey & Cole adopted $f = 0.5$, identifying the time at which the most massive progenitor is 50 per cent of the present-day mass as the nominal point at which haloes are born, while Viana & Liddle (1996), looking specifically at the mass–temperature relation for galaxy clusters, use a value of $f = 0.75$. Note that in any of these models, the dependence on the power spectrum is only through $\sigma(M)$, the rms fractional density perturbation for the mass-scale M; the dependence on Ω_0 and h enters through the linear theory growth factor, through the spherical collapse physics, and through the star formation model (by fixing ages, baryon fraction, etc).

Fig. 1 depicts the distribution of formation redshifts for haloes of $10^{12}\,M_\odot$ both for the S distribution and for the LC distribution with f values of 0.5, 0.75 and 0.9 for comparison. These results assume a *COBE*-normalized ΛCDM model with $\Omega_0 = 0.3$, $\Omega_\Lambda = 0.7$ and $h = 0.65$ (yielding, in this case, a mean peak height of $\nu = 0.69$ and $\sigma_8 = 1.08$). Note the large width of the S distribution, peaking at $z \sim 1.0$, but with a significant tail extending out to $z \sim 4$–5 and appreciable ongoing formation today. By contrast, LC distributions with larger values of f produce much narrower distributions, which peak at lower redshifts and fall more rapidly to high z.

[6] This ambiguity arises because in the excursion-set formalism, one follows a random walk of trajectories of the spatially filtered δ to the first up-crossing above some threshold value. The 'tagged' mass is statistically defined as the expectation value for the mass of a halo in which a given particle will end up, but this will in general differ from the actual mass in a given realization. This ambiguity can lead to predictions of negative probability densities at $z \sim 0$ in models with primordial power-spectrum indices $n > 0$.

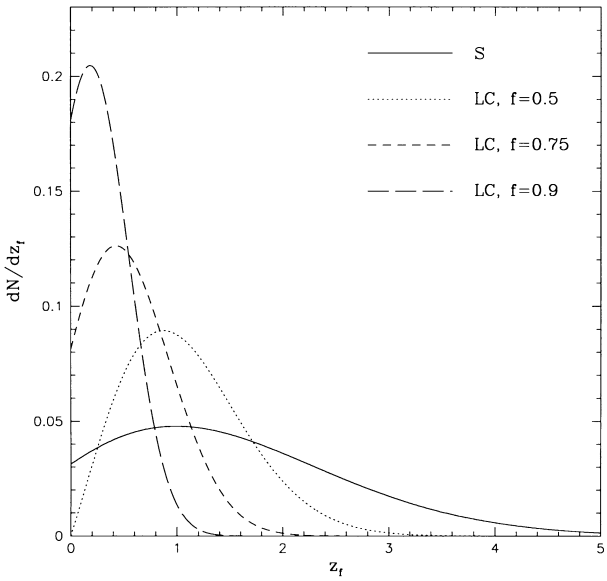

Figure 1. Formation redshift distribution for the S distribution (solid line) and for the LC distribution with $f = 0.5$, 0.75 and 0.9 (dotted, short-dashed and long-dashed lines, respectively), assuming a ΛCDM model with $\Omega_0 = 0.3$ and $h = 0.65$. Note the appreciable width of the S distribution and the decreasing width and peak z_f values for LC distributions with increasing f.

2.4 Spin distributions

Assuming constant specific angular momentum, the disc scale-length can be related to λ, the spin parameter of the halo (e.g., Mo et al. 1998),

$$R_d = \frac{\lambda G M}{\sqrt{2} V_c^2}, \tag{12}$$

fixing the initial surface density of the gas and thus affecting the SFR, luminosity and surface brightness. Therefore, it might be supposed that the predicted TF relation and other properties would depend sensitively on spin. HJ99 considered only fixed values for λ, rather than accounting for its detailed distribution. The spin distribution is usually taken to be log-normal centred at $\lambda \sim 0.05$, as indicated by numerical simulations. However, as is the case for the formation redshift distribution, heuristic arguments suggest that the distribution of spin parameters should depend on the mass, the formation redshift and possibly on the cosmological parameters and/or power spectrum. If so, the effect of scatter in the spin parameter on the TF relation could be different from that inferred from numerical simulations.

Heavens & Peacock (1988) calculated the distribution of tidal torques acting on matter in the vicinity of mildly non-linear density maxima, assuming a spherical accretion model to calculate binding energies, and derived the resulting spin parameter distribution. They found an anticorrelation between peak height and spin parameter, but pointed out that the intrinsically broad range of the λ distribution swamped the systematic shift with peak height, ν, resulting in a fairly weak anticorrelation. Catelan & Theuns (1996) extended these results to obtain the joint probability distribution function (PDF) for spin parameters and peak masses using the distribution of peak shapes in different CDM models. They confirmed the broadness of the spin parameter distribution and the anticorrelation with peak height (which is essentially due to the fact that higher peaks will generally be more spherical and thus harder to spin-up). Their results, however, exhibit a systematic shift towards higher λ values than those of Heavens & Peacock, such that $\nu = 1$ peaks have rms λ values of $\sim$0.15, instead of 0.05, thus closer to the observed value of 0.5 for spirals. The anticorrelation conjecture has not been fully tested by simulations, but some support comes from Ueda et al. (1994). Lemson & Kauffmann (1999) argued against an environment-dependent λ. However, the environment was defined on a $10\,h^{-1}$ Mpc scale, and we do not expect strong correlation between the density field smoothed on galaxy scales and this large scale.

Since the indications for a distribution peaked at higher spins and an anticorrelation with peak height are good, but not yet well-established, we consider two models, with and without the joint distribution in λ and ν. For the former, we adopt the joint distribution function (Catelan & Theuns 1996)

$$P(\lambda|\nu) = \frac{0.68}{\lambda}\left\{1 + 0.02\left[\frac{\lambda}{\lambda_0(\nu)}\right]^4\right\}\exp\left\{-\frac{\log^2[\lambda/\lambda_0(\nu)]}{0.98}\right\}, \tag{13}$$

where $\lambda_0(\nu) = 0.11\,\nu^{-1.1}$ and $\nu = \nu(z) = \delta_c(z)/\sigma(R, z)$. Since, at a fixed epoch, there is not a one-to-one relationship between ν (defined for the spatially averaged overdensity field) and mass, owing to the distribution of halo shapes, equation (13) effectively corresponds to an average of ν over all shapes of a given mass.[7]

2.5 Chemical evolution

HJ99 assumed the stellar populations to have constant metallicity fixed at the solar value for all time. More realistic models should, of course, account for chemical evolution. To study the effect of chemical evolution on the TF relation, we assume that galaxies are (chemically) closed boxes, for which analytic results for the evolution of metallicity exist (e.g., Pagel 1997). This assumption seems to be justified by the detailed hydrodynamical computations of a multiphase ISM by MacLow & Ferrara (1999).

Our chemical evolution model is thus as follows. Let M_s be the mass of the galaxy in stars, M_g be the mass in gas and Z be the fractional abundance of metals. We invoke the instantaneous recycling approximation (IRA), such that the gas produced by stars is immediately returned to the ISM, which is therefore enriched primarily by metals from short-lived massive stars. Defining b as the fraction of the mass turned into stars in each generation that is returned instantaneously from short-lived massive stars, y as the fraction of gas converted into metals by supernovae and f as the fraction of gas that is returned by stars and remains in the galaxy (i.e. it is not expelled from the galaxy by supernova winds), then

$$\frac{\mathrm{d}(ZM_g)}{\mathrm{d}M_s} = \frac{Z}{1-b} + yf + \frac{bZf}{1-b}. \tag{14}$$

Equation (14) is simply the conservation of metals; the terms on

[7] We point out that the binding energy used to calculate λ is derived using a spherical accretion model, but that for the lower, more irregular peaks, this is probably only a lower limit to the actual binding energy, resulting in an underestimate of λ. Combined with the arguments above from Catelan & Theuns (1996), one can push the predicted spin values for spirals (if these are indeed associated with lower-ν peaks, as opposed to ellipticals, which are associated with higher peaks) closer to the observed values, such that one need not rely as heavily on dissipation to spin-up spirals.

the right-hand side respectively represent the metals lost to the gas in making stars, the metals gained from supernova debris and the metals returned unprocessed.

If we assume now that the galaxy is a closed box, such that $f = 1$ and $M_g = M_{g0} - M_s$ (where M_{g0} is the initial gas mass), then $Z = Z_0 + y \ln(1/f_g)$, where f_g is the gas fraction of the disc. Of course, iron is not produced by supernovae of massive stars, but rather in Type Ia supernovae, which typically onset after 1 Gyr or more. Oxygen, on the other hand, *is* mostly produced by short-lived massive stars, and the IRA is thus an excellent descriptor in this case. In order to account reasonably for the evolution of iron, we adjust the yield to reflect the delay in its production by simply taking a value of 0.03 for the geometric mean of the yields from Type II and Type Ia supernovae. We also set the zero-point redshift dependence of the metallicity so as to comply with observations of damped Lyman-α systems, which suggest that the ISM is already enriched up to a certain metallicity at a given redshift. Adopting the relation found by Pettini et al. (1999; see fig. 8 therein), we thus have that the metallicity, Z, evolves with redshift, z, as

$$Z(z; z_f) = 0.03\, Z_\odot \ln\left[\frac{1}{f_g(z; z_f)}\right] + 0.28\, Z_\odot 10^{-0.25z}, \qquad (15)$$

where the solar metallicity $Z_\odot = 0.02$, $f_g(z, z_f)$ is the gas fraction of the disc whose age is given by the time elapsed between z_f and z, and the last term gives the zero-point metal enrichment as a function of redshift. Of course, f_g and thus Z also generally depend on Ω_0, h, M, m_d and λ as per equation (3). It will be shown that chemical evolution will be an important factor in reducing the predicted scatter in the TF relation.

2.6 Summary of the model

To recap, our galaxy model is built as follows. For a given halo mass in the assumed cosmogony, we draw z_f from either the S or LC distribution. The peak height is computed and λ is then drawn from the joint distribution in peak height and spin. Equations (5) and (12) are used to calculate the circular velocity and disc scalelength, respectively. The empirical Schmidt law above is used to calculate the SFR and remaining gas fraction as functions of time, according to equations (2)–(4), as in HJ99. With an assumed IMF and the above prescription for chemical evolution, the spectrophotometric stellar evolution code is then used to derive broad-band magnitudes.

3 RESULTS

We first study the respective impacts of the various ingredients that have entered into our galaxy formation model. In Figs 2 to 12, we illustrate examples of how our predictions for the TF relation in the *B*, *R*, *I* and *K* bands change as the model inputs are varied. These results will allow the reader to infer how the predictions of any of our models, or any other models that appear in the literature, would change with different input physics or assumptions. In each graph, the solid line delineates the power-law fit to the TF prediction (along with 1σ errors given by the dashed lines and denoted in each plot by 'σ') and the four 'scatter-point curves' trace the spread in the predicted TF relation for four fixed masses (10^{10}, 10^{11}, 10^{12} and $10^{13}\,M_\odot$), using $\sim$150 points each.

Overplotted on each graph are open symbols representing data from Tully et al. (1998). These data, comprising spiral galaxies in the loose clusters of Ursa Major and Pisces, represent one of the most carefully defined TF samples. The inclination-corrected full width at half-maximum (FWHM) of the lines has been converted to W_R^i, which approximates to $2V_c$, and the data have been corrected for dust extinction. The scatter in the *B*, *R*, *I* and *K* bands is 0.50, 0.41, 0.40 and 0.41 mag, respectively. While many authors compare their models to TF data by defining a 'fundamental' TF relation derived from the particular data set in question, we argue that, given the observational selection effects inherent in defining such samples, there is no particular significance or accuracy associated with any one determination of the slope and normalization of the TF relation. Instead, we examine how well these data fit to our model, in a χ^2 sense, using the measured scatter as an estimate of the error associated with each point. For each plot we calculate the resulting χ^2 and denote by 'p' the probability of obtaining this large a value of χ^2 given that the model is correct; values of p below 10^{-3} are listed as zero. In addition, since the data have excluded spirals which show evidence of merger activity or disruption in the form of starbursts, we exclude from our model galaxies those having $B - R < 0.3$.

The models in Figs 2 to 12 are designed to provide a qualitative feel for the nature and degree of variation in our predictions as different input assumptions are altered, and do not attempt to fit any data. Though the results of these investigations are highly informative, the reader may wish to proceed to Section 4 for a discussion of models aimed at matching TF and other observational data.

3.1 Formation redshift distribution

3.1.1 S distribution

As discussed above, the distribution of formation redshifts should lead to some scatter about the TF relation, and Fig. 2 illustrates this effect using the S distribution. We show results for two cosmogonies to indicate the dependence of the results on some of the cosmological parameters. The left-hand panels of Fig. 2 depict the results for the S distribution of z_f in an EdS universe, while the right-hand panels show the results for a flat, Λ-dominated universe. Here, and unless otherwise indicated, we shall take EdS models to have $h = 0.65$, a power-spectrum shape parameter[8] $\Gamma = 0.2$, and an rms density contrast fluctuation over $8\,h^{-1}$ Mpc spheres of $\sigma_8 = 0.5$. For ΛCDM models, we assume $\Omega_0 = 0.3$, $h = 0.65$ and a *COBE*-normalized power spectrum (Bunn & White 1997) with $\Gamma = \Omega_0 h = 0.195$. For all cosmogonies we assume $\lambda = 0.05$, a fixed metallicity given by the solar value ($Z = Z_\odot$), and a Salpeter IMF, $\mathrm{d}\log N_*/\mathrm{d}\log M_* = -\alpha$ with $\alpha = 1.35$, all unless otherwise indicated. We vary these assumptions individually in order to assess the impact of different ingredients of the model. Thus, the distribution of spin parameters is not taken into account unless specifically stated.

To understand the results, we begin by examining the predictions for the *K*-band TF relation in the ΛCDM model. Here we find that the spread in z_f translates directly into a spread in V_c (with earlier formation implying higher circular velocity), which widens for lower masses, since these can form over a broader range of redshifts stretching back to higher z. This

[8] Since values of $\Omega_0 h \gtrsim 0.3$ already seem to be ruled out (e.g. Peacock & Dodds 1994), Γ in the case of EdS models is defined simply as a fitting parameter in the CDM transfer function. In the case of ΛCDM models, we formally take $\Gamma = \Omega_0 h$.

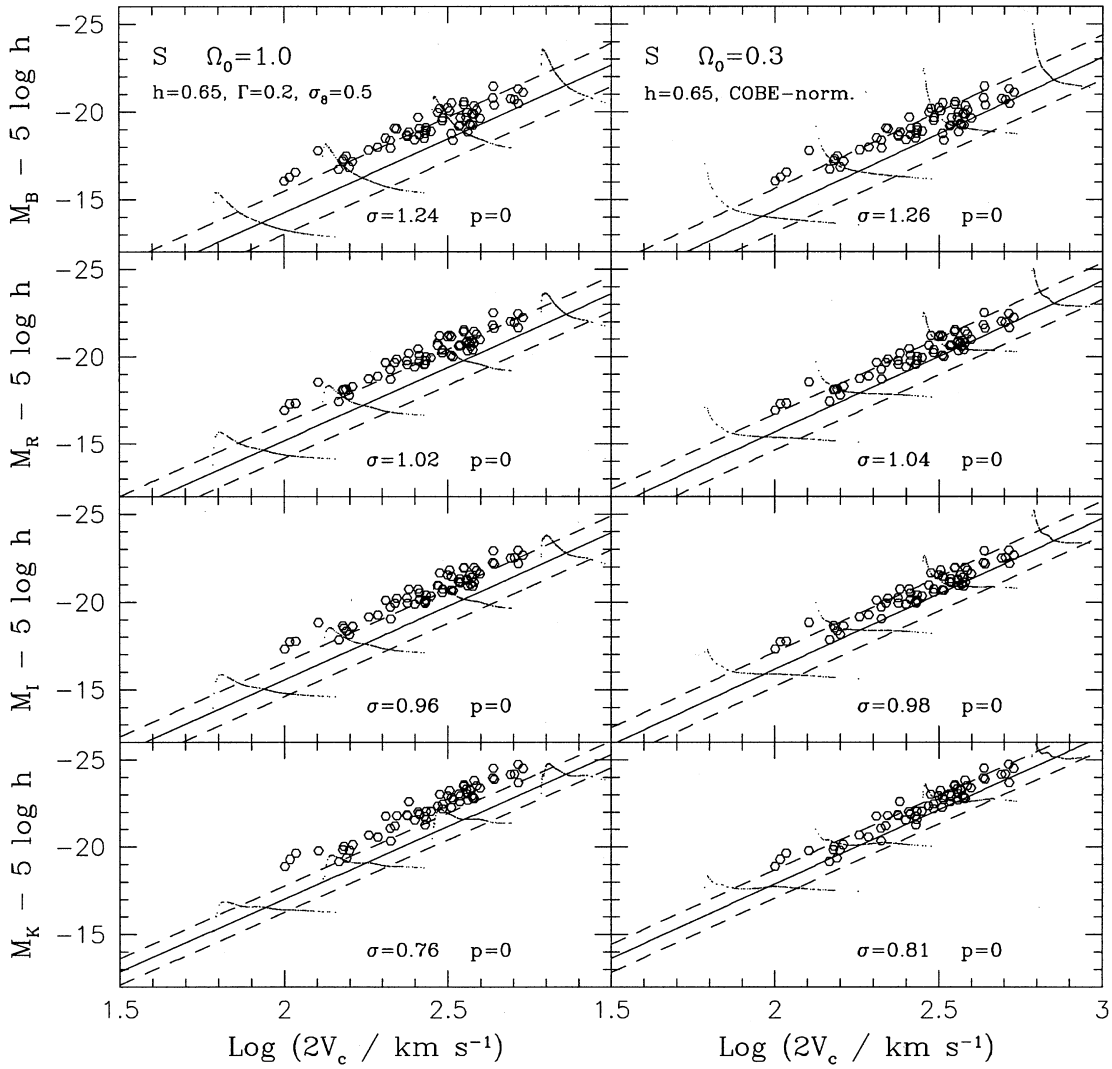

Figure 2. S-distribution predictions. The left panels show the predictions for the present-day TF relation in B, R, I and K for the S distribution assuming an EdS universe with $h = 0.65$ and a CDM power spectrum with $\Gamma = 0.2$ and $\sigma_8 = 0.5$. The right panels display the results for a *COBE*-normalized ΛCDM model with $\Omega_0 = 0.3$, $h = 0.65$ and $\Gamma = \Omega_0 h$. Both assume a Salpeter IMF, a constant spin parameter of $\lambda = 0.05$ and constant metallicity fixed at the solar value. The model predictions for haloes of mass 10^{10}, 10^{11}, 10^{12} and 10^{13} $M_\odot$ are indicated by the four 'scatter-point curves' in each panel, and the solid lines are the fits to these predictions, with 1σ errors indicated by the dashed lines. The open symbols are data from Tully et al. (1998). Note that the EdS model, in particular, underpredicts the luminosity in all bands.

broadening of the TF with lower V_c arises generically from a realistic formation distribution and is observed in most TF samples. The predicted M_K, however, varies very little for galaxies of a given mass; this wavelength primarily reveals the light from giants, which, for a sufficiently evolved galaxy, serves as a faithful tracer of the total luminous mass, regardless of the precise age of the galaxy. At higher masses, which collapse later, we see the TF spread for a fixed mass turn upwards for the most recently formed objects. These objects are sufficiently young that even the K-band light is sensitive to their ages, with younger objects being brighter.

As we go to bluer bands, which trace younger populations, this effect becomes more dramatic; we find that, for a given mass, younger galaxies become substantially brighter, increasing the spread in the TF relation. This is a simple consequence of equations (2) and (3), which state that the SFR and remaining gas fraction are highest at the time of formation and rapidly decline with age (see fig. 1 in HJ99). There is a competing effect, however, from the fact that galaxies that are too young will not have had enough time to convert much gas into stars and so will become dimmer. For this reason, our plots often outline a peak magnitude for galaxies of a given mass, in those cases where the z_f distribution produces a large fraction of very young galaxies, as seen for the S-distribution EdS model in the left-hand panels of Fig. 2. Galaxies on the young side of this magnitude peak have formed so close to the epoch of observation that even a relatively small increase in their age can substantially increase their stellar luminosity. Such galaxies would likely exhibit the properties of starbursts and be excluded from carefully defined TF samples. Indeed, model galaxies removed by our colour selection criterion ($B - R < 0.3$) tend to include those on the younger side of these peaks. In general for our models, the distribution in z_f is thus found to be the primary source of scatter in the TF relation. At low mass, more recently formed objects of a fixed mass scatter to lower V_c at roughly constant magnitude in K, while in the case of higher masses and/or bluer bands, the scatter is coupled both to higher V_c and to higher luminosity.

Overall, these S-distribution predictions do not fit the TF data in any waveband, as the models are too faint in every case and the predicted scatter here is too large by about 0.7 mag in B and 0.3 mag in K. This problem is due largely to the fact that the S distribution has a substantial high-redshift tail producing older, fainter galaxies with high V_c. Thus, if we assume star formation proceeds passively according to a Schmidt law, TF observations imply that *the majority of present-day discs could not have formed much beyond a redshift of* 2–3. Thus, the spread in the TF relation can be an important tool in understanding the star formation history of galaxies (Buchalter, Jimenez & Kamionkowski, in preparation).

3.1.2 LC distribution

Fig. 3 depicts corresponding results for the same parameter choices, but using the LC distribution with $f = 0.75$. This distribution has both a lower peak value of z_f and a smaller FWHM than the S distribution (see Fig. 1), producing significantly less scatter in the predicted TF relations and a larger fraction of younger galaxies, as compared with Fig. 2. Despite the smaller scatter, these models still do not fit the observed TF relation in the various bands. Note that the EdS model here actually yields excellent agreement in B, but predicts galaxies that are too faint in I and K.

In Figs 4 and 5 we examine LC distributions with values of $f = 0.5$ and $f = 0.9$, respectively. Lacey & Cole (1993, 1994) found that the statistics of the time at which present-day haloes accreted half their mass (i.e. $f = 0.5$) provides an excellent fit to the results of N-body simulations. Here we see that the $f = 0.5$ ΛCDM model provides an excellent fit to the K-band TF relation, marginal fits in I and R, but predicts galaxies that are too faint in B, thus highlighting the importance of using multiwavelength constraints. This model also produces TF scatter that is about 0.1–0.4 mag too large, going from K to B. The EdS predictions are again too faint in every case. In general, we find that LC distributions with plausible values of f fare better than S distributions at matching TF data, suggesting disc formation in the range $0 < z < 3$ (see below).

The $f = 0.9$ models have a z_f distribution which produces galaxies only in a narrow interval centred at low redshift (see Fig. 1). These young galaxies produce an extremely tight TF relation in the EdS case, in part because effectively no galaxies form above a relatively low maximum redshift of $z \sim 1$, but also because many of these recently formed galaxies fall on the young side of the magnitude peak and are excluded by our colour

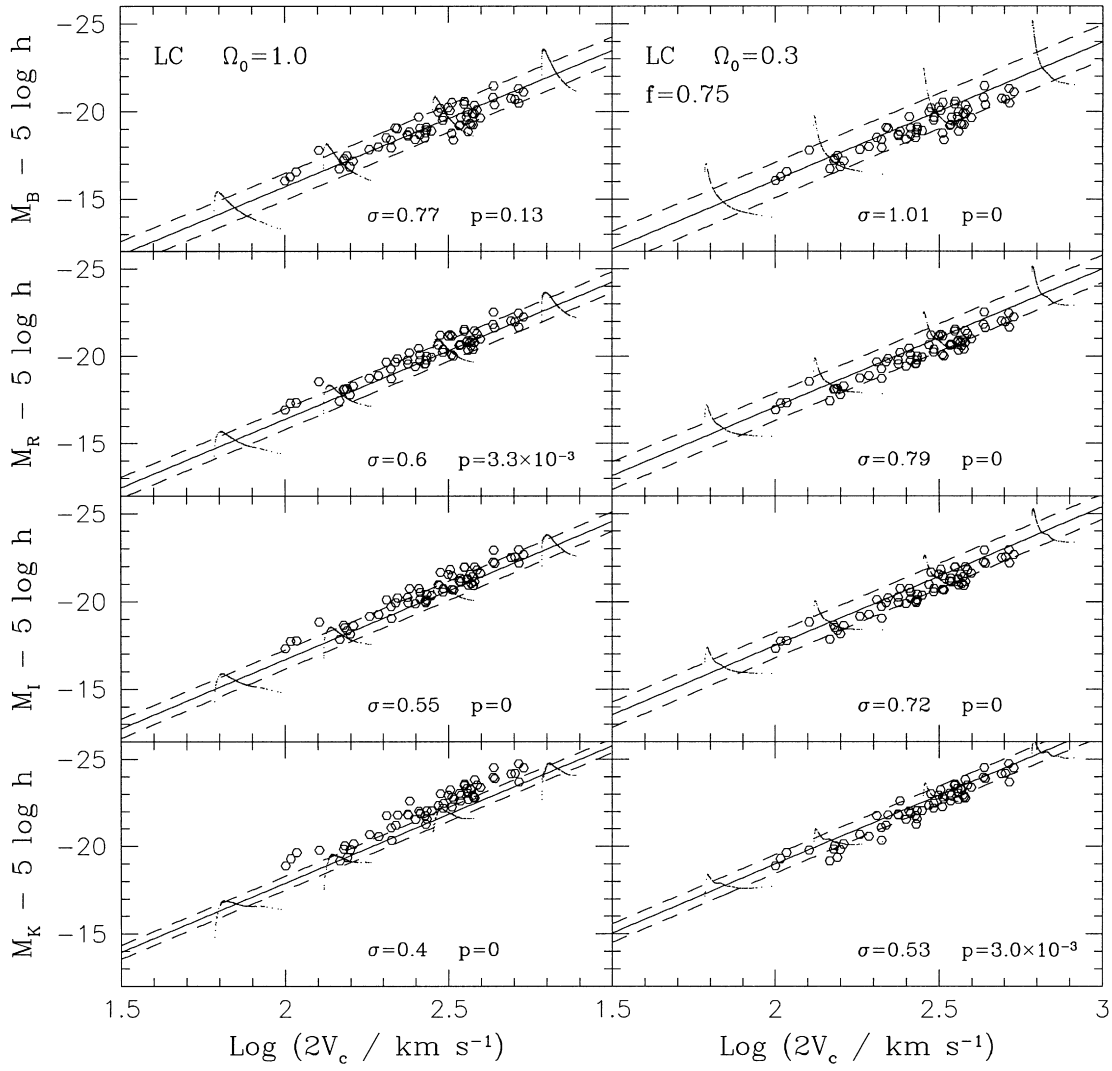

Figure 3. LC-distribution predictions. Same as Fig. 2, but using the LC distribution with $f = 0.75$.

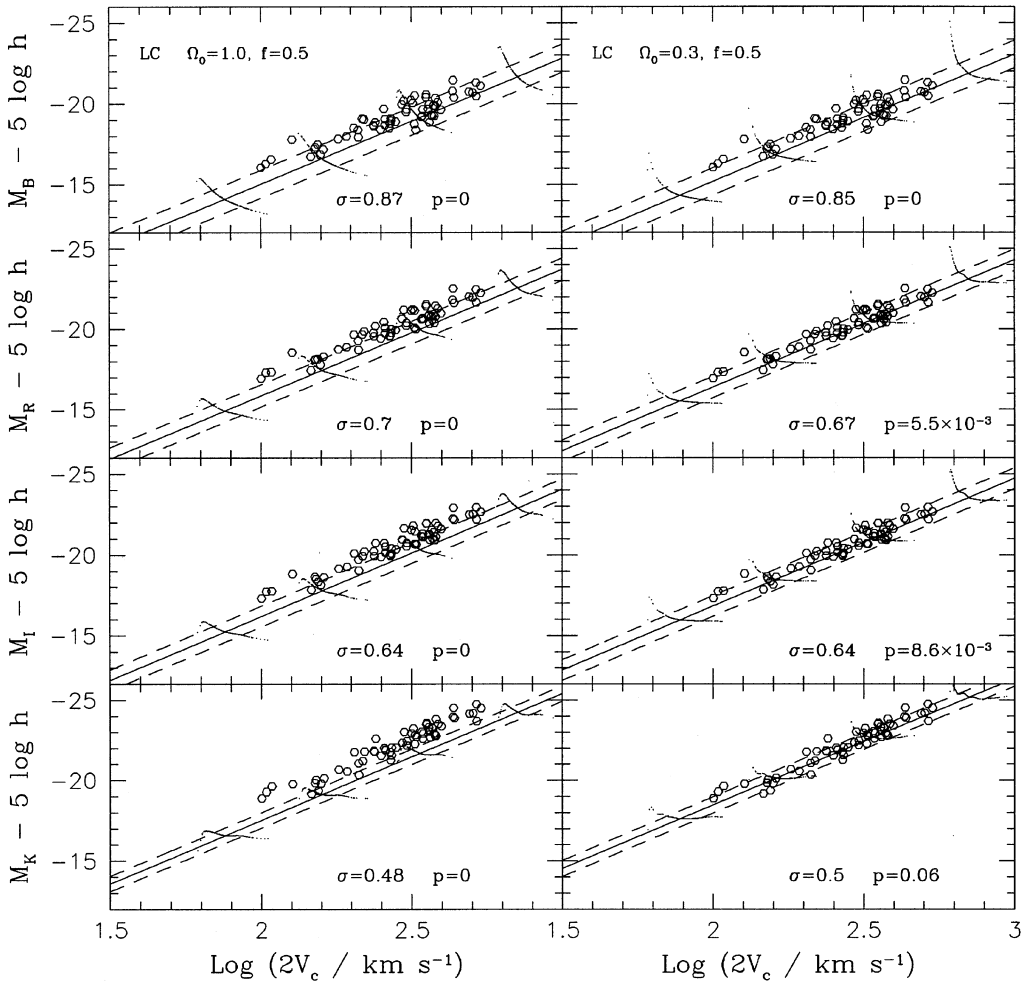

Figure 4. Same as Fig. 3, but using $f = 0.5$. Note how the Λ model yields excellent agreement in *K*, marginal agreement in *R* and *I*, and a statistically poor fit in *B*.

selection. In effect, this z_f distribution has 'pushed' galaxies over to the faint side of the magnitude peak, where their colours resemble those of starbursts, and the low scatter is due to the small number of galaxies 'older' than the peak, particularly in *K*. Thus, while the intrinsic TF scatter of all galaxies in this model is higher than the fits indicate, the measured scatter, based on observational selection, can be quite low, and this effect is important when considering recently formed populations. This effect is less exaggerated in the ΛCDM case, where discs at a given redshift are older, so that fewer will fall on the young side of the magnitude peak.

Irrespective of the scatter, however, the $f = 0.9$ models fail to fit the TF slope and normalization. For the reasonable cosmological parameter values in the right-hand panels, the predicted galaxies are very young and thus excessively bright. Thus, TF constraints also imply that *the majority of disc formation cannot have happened at* $z < 1$. Of course, from a physical standpoint, such large values of f are anyway unreasonable. Note that, even with $f = 0.9$, the EdS model still produces galaxies that are too bright in *B* and too faint in *K*, despite yielding excellent agreement in *I* and *R*, again highlighting the importance of multiwavelength constraints.

3.2 Dependence on cosmogony

3.2.1 Power-spectrum shape and amplitude

In Fig. 6 we explore the impact of individually changing the shape and normalization of the power spectrum, using the S distribution in an EdS universe. In the left (right) panels we adopt $\Gamma = 0.5$ ($\Gamma = 0.2$) and $\sigma_8 = 0.5$ ($\sigma_8 = 1.0$). In both cases, the resulting galaxies are several magnitudes too faint and produce dramatically larger scatter in their TF relation. In the case of higher σ_8, haloes of a given mass will be smaller and correspond to rarer peaks. These collapse at earlier times, leading to larger V_c and older, dimmer galaxies. Extending the range of collapse redshifts back to higher z also substantially increases the scatter. Similarly, in these CDM models, increasing Γ shifts more power to smaller scales ($R \lesssim 10$ Mpc), leading to the same result. Though we do not explicitly explore variations with n, it can be inferred that values of $n > 1$, which also tilt power towards smaller scales, will have a similar effect. Conversely, values below unity might lead to better agreement with the data, but there are already strong constraints on the tilt (e.g. Kamionkowski & Buchalter 2000).

3.2.2 Hubble constant and matter density

Given the uncertainties in our present understanding of galaxy formation, it makes little sense to attempt to constrain cosmological parameters using TF data. Rather, with these parameter values dictated by other, more direct tests, we should employ the TF relation to gain insight into the details of galaxy formation. Variations in Ω_0 and h affect almost every aspect of the model,

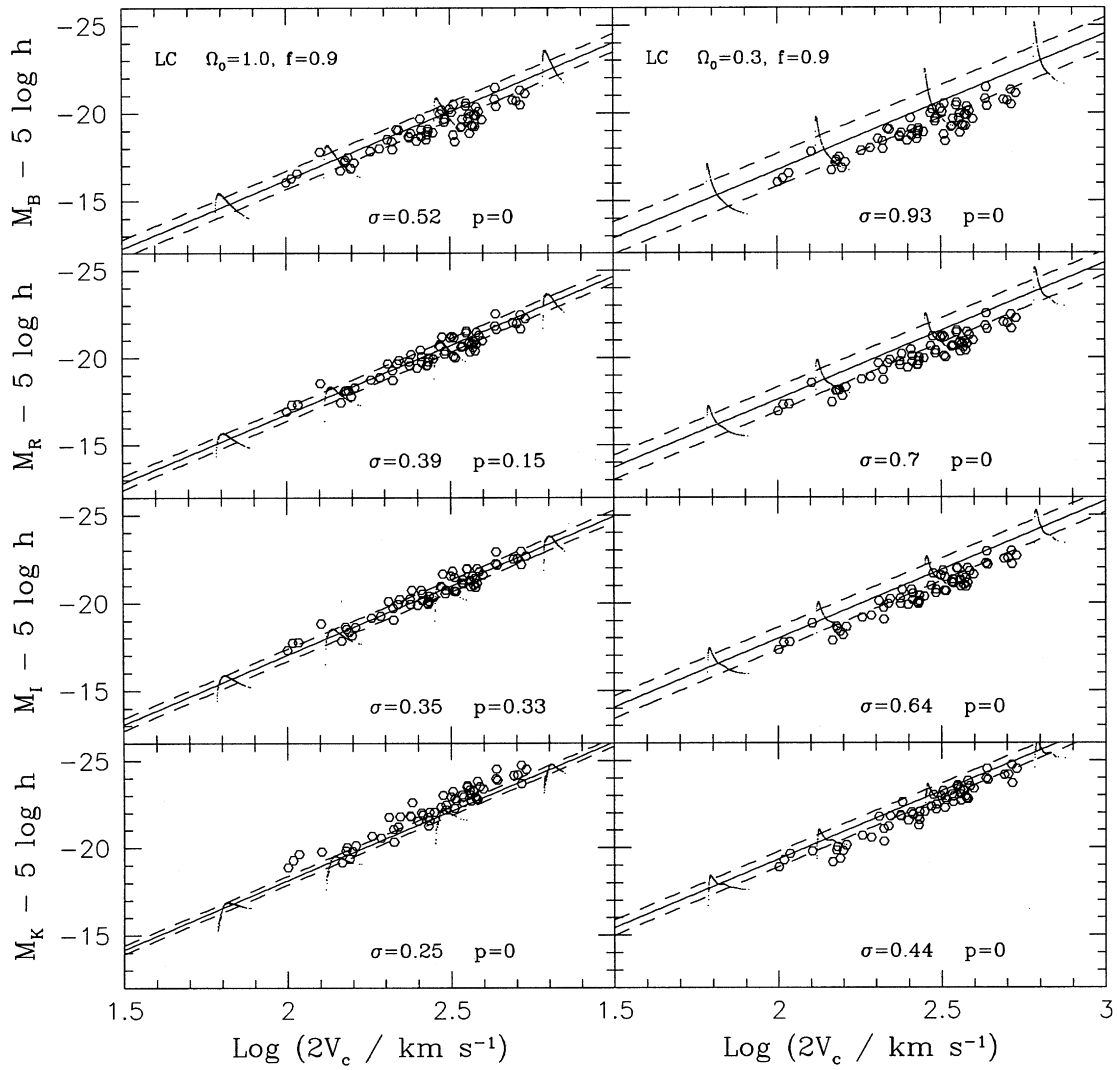

Figure 5. Same as Fig. 3, but using $f = 0.9$. In this case, all discs form fairly recently and many fall on the younger side of the magnitude peak. In the EdS case in particular, these effects combine to yield very little TF scatter for the few relatively older galaxies that fall redward of our colour selection criterion.

such as the disc mass fraction, galaxy ages and circular velocities, star formation rates and the power-spectrum shape. In Figs 7 and 8 we plot S distributions with $h = 0.5$ and $h = 0.75$, respectively. Little change is seen in the EdS cases, while for low Ω_0 the net result appears to be that lower (higher) values of h produce galaxies that are brighter (fainter). Changes in h do not, however, strongly affect the scatter. Note that the $h = 0.5$ ΛCDM model provides reasonable agreement in K, I and R, but is not successful in B. The dependence of the models on Ω_0 can be gleaned from comparing the left- and right-hand panels of the various figures. In general, for a fixed halo mass, lower values of Ω_0 will yield a larger disc mass and thus brighter luminosity. We have seen repeatedly that high values of Ω_0 invariably predict galaxies that are excessively faint as compared to observations.

In order to gain broader insight into the viability of the model with respect to cosmological parameters, we generated data for the $\Omega_0 = 1$ case with $\Gamma = 0.2$ and $h = 0.45$–0.75, and for $\Omega_0 = 0.2$–0.5 cases with $\Gamma = \Omega_0 h$ and $h = 0.55$–0.75, both for the S distribution and for LC distributions with $f = 0.5$ and 0.75. All were *COBE*-normalized. Only a handful of these models produced values of $p > 0.001$ in any band, and those which did invariably had values of $\Omega_0 h \sim 0.2$, as required by current measurements. EdS models generally produce galaxies that are too faint, unless unacceptably low values of h are adopted, and produce too large a scatter, unless unacceptably low values of σ_8 are adopted. The best-fitting models, in terms of both p and scatter, were LC distributions with *COBE* normalization, $\Omega_0 \sim 0.3$ and $h \sim 0.65$, similar to the best-fitting values obtained in earlier work (EL96; van den Bosch 2000; Firmani & Avila-Reese 2000) and in agreement with current estimates. As mentioned above, the S-distribution predictions are generally too faint, because of the significant fraction of older galaxies arising from the high-redshift tail.

In looking at the overall variation in TF predictions with respect to the variable input assumptions investigated in this work, it is found that the cosmological and power-spectrum parameters have a strong impact on the slope, normalization and scatter of TF predictions. In particular, though we do not pay close attention to the precise results of the various 'exploratory' illustrations presented in Figs 2 to 12, we point out that in all cases investigated, the fitted TF slope for a given model is very nearly constant across all wavebands. The normalizations vary in accordance with the amount of light predicted to fall in various parts of the spectral energy distribution of our stellar populations, but the relative constancy of the slopes within a given model

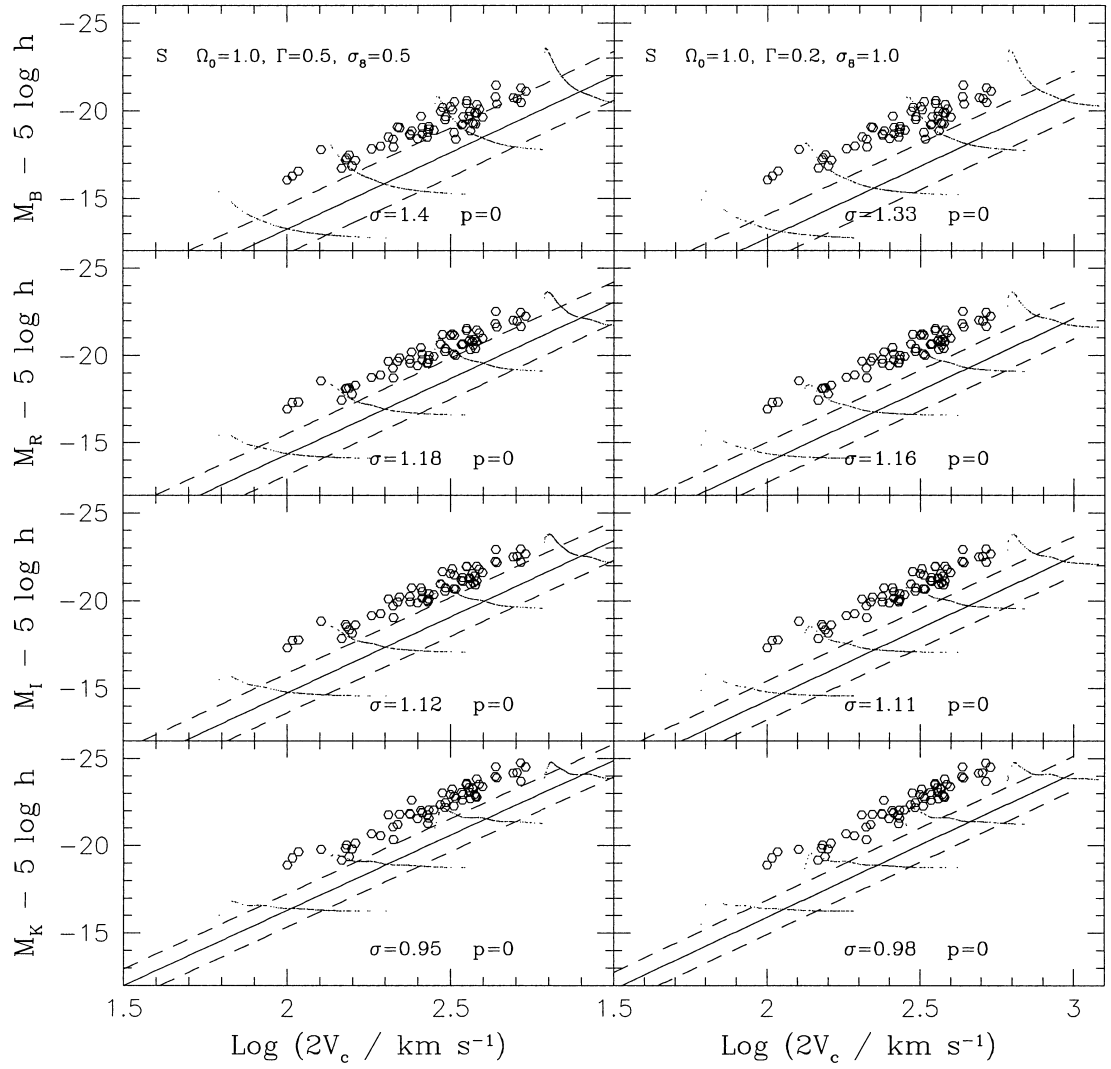

Figure 6. Dependence on the power spectrum shape and amplitude. TF predictions for the S distribution in an EdS universe for $\Gamma = 0.5$ and $\sigma_8 = 0.5$ (left panels) and for $\Gamma = 0.2$ and $\sigma_8 = 1.0$ (right panels). Comparing with Fig. 2, we find that high Γ and high σ_8 both lead to earlier collapse, producing fainter discs with a much larger TF scatter.

reveals that the TF relation is mainly a reflection of the particular mass–circular velocity relation of that model, which in turn depends on the cosmogony and formation redshift distribution.[9] In other words, the TF relation is found to arise largely as an imprint of gravitational evolution upon cosmological initial conditions, as other workers have concluded (EL96; Firmani & Avila-Reese 2000). Star formation and chemical enrichment, however, are found to play a key role in fixing the precise luminosity properties and bringing predictions in line with the actual data.

3.3 Spin parameter distribution

We now turn to the issue of the spin parameter distribution. Figs 9 and 10 correspond to the S and LC distributions from Figs 2 and 3, but with the joint probability distribution in λ and ν now taken into account. This additional degree of freedom naturally spreads out the distribution of points predicted for each mass, which no longer trace a one-dimensional spread as in previous figures. This smearing is particularly large in B, since changes in spin will alter the gas density and thus SFR, to which bluer bands are more sensitive. Looking at the S distribution in Fig. 9, we find that the TF scatter in every case is roughly similar to, but less than, that in Fig. 2; the broadening has aligned roughly along the TF relation itself. This arises from the fact that, for a given mass, older systems which collapse earlier and have higher V_c will tend to have lower spins, and thus higher gas surface densities and SFRs, and higher luminosities, scattering them upwards in the TF plane towards the mean TF relation. Conversely, the younger low-V_c systems, which correspond to lower peak heights and thus higher spins, will have lower luminosities, also scattering on average closer to the mean TF relation. This twisting of the distribution of points for a given mass towards the mean TF relation will be more dramatic in the B band owing to the higher sensitivity to small changes in the SFR. Thus, the net effect of the λ–z_f anticorrelation is to scatter objects roughly along the TF relation, tightening the overall spread somewhat, particularly in bluer bands.

A similar result is found in the LC case, though here the z_f distribution is weighted towards more recent epochs, exaggerating

[9] Observational effects, such as the presence of dust, could alter the observed TF slope in different bands, as discussed by Avila-Reese & Firmani (2000a).

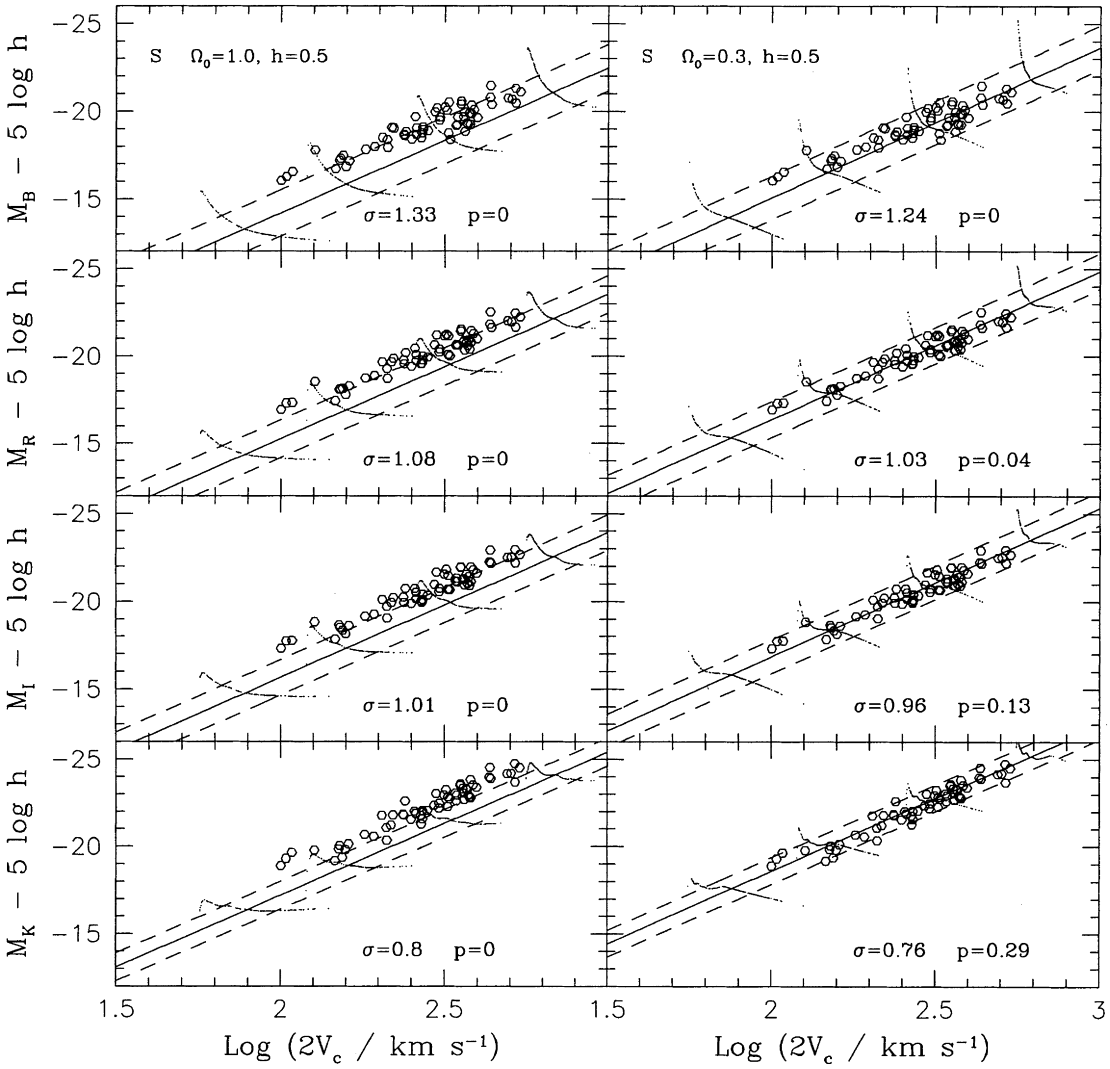

Figure 7. Dependence on the Hubble constant. Same as Fig. 2, but using $h = 0.5$. The resulting changes in baryon fraction and age lead to a brightening of the TF relation, particularly for low Ω_0.

this effect and leading to a larger systematic reduction in the scatter, once our colour selection criterion is enforced. Thus, in practice, accounting for the joint probability distribution in λ and ν can reduce the TF scatter by about 0.15 mag in B to 0.05 mag in K, for some plausible cosmogonies. Otherwise, the spin distribution does not have a great impact on the TF relation, as was also concluded by Firmani & Avila-Reese (2000). As a corollary to this, we find that high surface brightness and low surface brightness discs, as distinguished by different λ or R_d in our model (see Fig. 15), are predicted to lie on the same TF relation, as is in fact observed (Zwaan et al. 1995; Sprayberry et al. 1995; Tully et al. 1998). Also note in Fig. 10 how the predictions yield excellent agreement in B for the EdS case and in K for the ΛCDM case, but not in any other waveband.

The fact that the spin distribution does not have a very large effect on the scatter of the local TF relation might at first seem to imply that the remaining gas fractions are independent of λ, in contrast to the observed correlation between surface brightness and gas fraction (e.g. McGaugh & de Blok 1997). Several important points serve to address this issue. First, the spread in spin parameters *does* alter the predictions at a fixed V_c by as much as a magnitude in B (note that the vertical scale in the figures spans almost 15 mag) but the anticorrelation with peak height tends to downplay this effect, since the effect tends to align along the TF relation itself. Secondly, the assumed Schmidt law is very efficient at converting gas into stars, so that on average we find lower typical values of f_g for local discs than found by McGaugh & de Blok (1997). Though the Schmidt law implicitly includes supernova feedback, it does not account for gas returned to the ISM by stars, which could increase f_g by $\sim$0.1 or more. Alternatively, the addition of a volume–density threshold criterion for star formation could also serve to delay the rapid consumption of gas and reduce the star-forming efficiency. The key point, however, is that even if our values for f_g were increased by 0.2, the main effect would be to make later-collapsing objects, which have higher spins and lower SFRs on average, less luminous; older objects with higher star-forming efficiencies would likely have had time to process the excess gas and thus be little changed at $z = 0$. The bottom line is that even a correlation as strong as that observed by McGaugh & de Blok (1997) between surface brightness and gas fraction would still not greatly alter the TF scatter. In fact, we *do* observe the correct trend between surface brightness and gas fraction, in the sense that, for early-forming and evolved objects, lower surface brightness correlates with

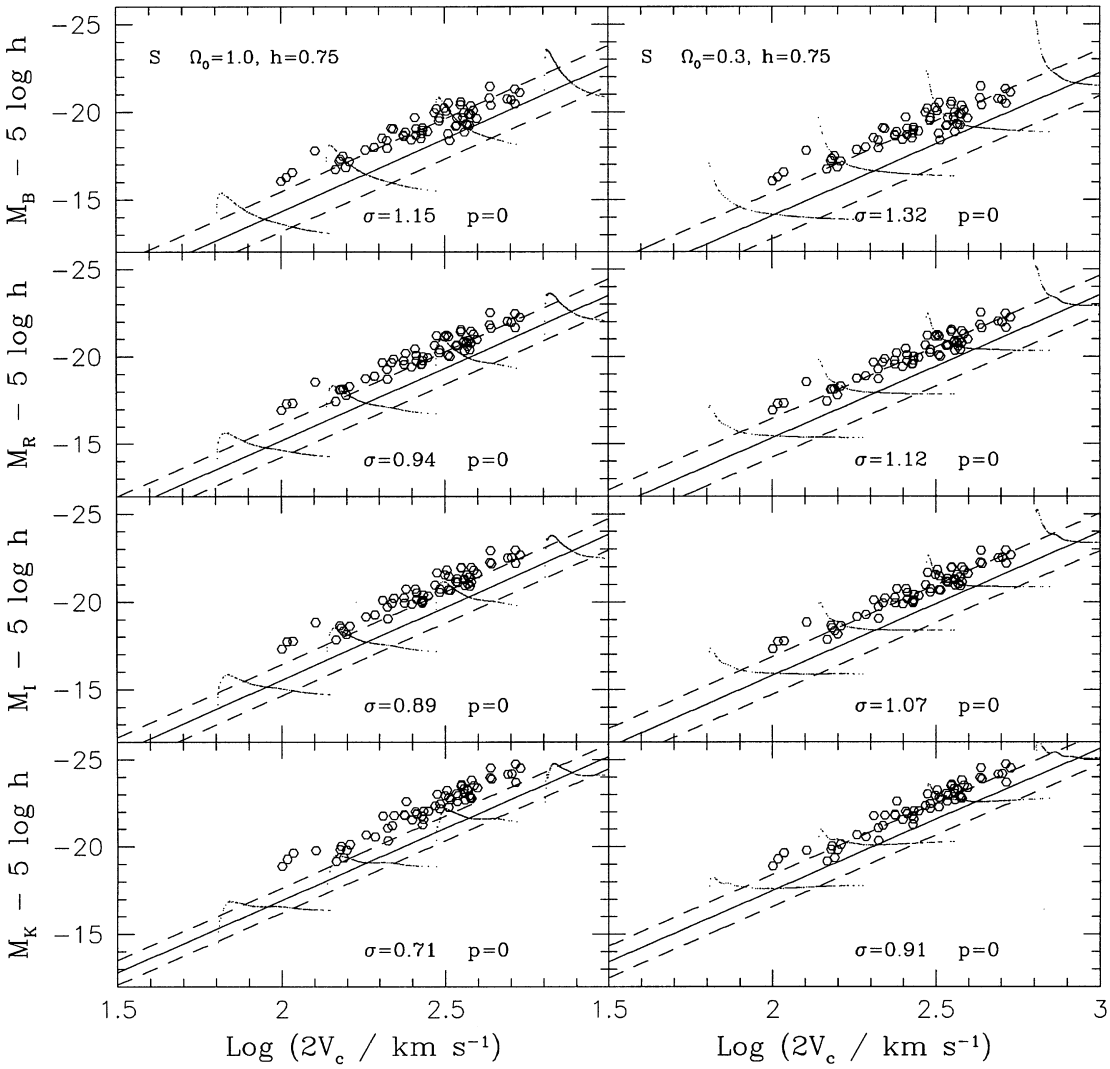

Figure 8. Same as Fig. 2, but using $h = 0.75$.

higher f_g (albeit the absolute values we obtain for f_g are somewhat low). The trend is weakened, however, by the presence of earlier-forming objects, which have high SFRs and can be very bright despite their high gas fractions. The issue of this and related correlations is discussed further in Section 4.2.

3.4 Chemical evolution and the IMF

The role of chemical evolution is investigated in Fig. 11 for the $\Omega_0 = 1$ S distribution and the ΛCDM LC distribution. Compared with their constant, solar-metallicity counterparts in Figs 2 and 3, these models have TF scatters that are systematically smaller by about 0.1 mag in all wavebands. This simply results from the fact that, relative to constant-metallicity systems, older discs (with higher V_c) will continually be forming populations of higher metallicity and thus have a higher integrated luminosity. Conversely, younger systems will be relatively dimmer, so that models with an evolving metallicity content will naturally align more tightly along a luminosity–circular velocity relationship than those with constant Z.

In Fig. 12 we examine the impact of changing the assumed IMF. The left-hand panels depict a Salpeter IMF with $\alpha = 0.95$ (denoted as Salpeter-2), while the right-hand panels represent a Scalo IMF (Scalo 1986), each for the ΛCDM LC distribution. Despite the fact that these IMFs both produce relatively more high-mass stars than the standard Salpeter IMF used to this point, the TF predictions are little changed; the Scalo IMF predictions are about 0.3 mag brighter on average, and the Salpeter-2 IMF predictions are almost identical to the standard Salpeter IMF. This is due to the fact that these systems are well evolved at $z = 0$, with little remaining gas to manifest the effects of the different IMFs. At higher redshifts, the effects would be more pronounced. Note that the Salpeter-2 model matches quite well in K, but not in any other band. This is yet another example of the importance of using multiwavelength constraints to discriminate between models that may appear to fit in a single band.

4 A MODEL THAT WORKS

4.1 The TF relation at $z = 0$ and $z = 1$

As an example of what can be accomplished with the theoretical framework presented here, we illustrate specifically the results for a *COBE*-normalized ΛCDM LC distribution with $f = 0.5$,

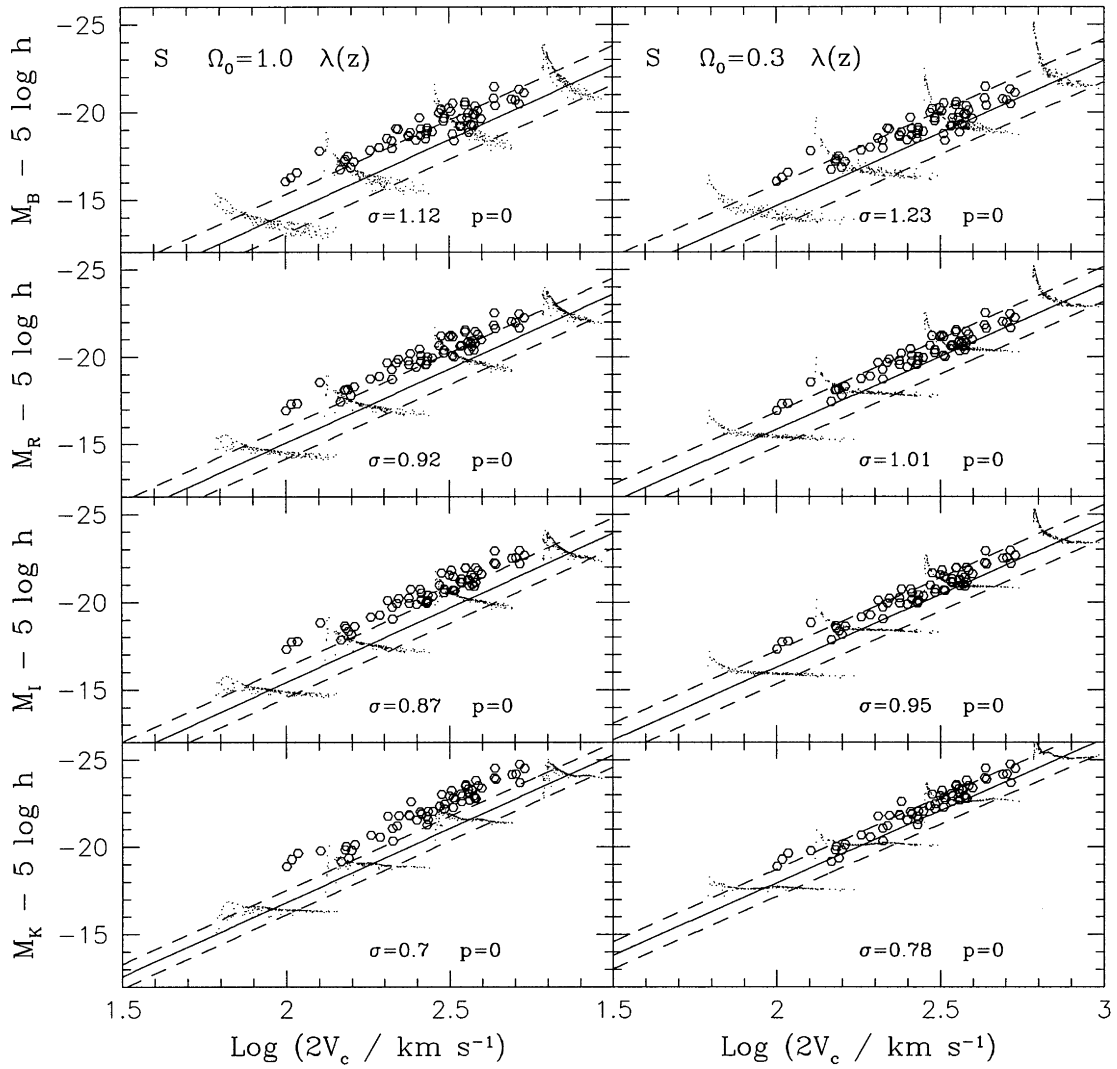

Figure 9. Effect of joint distribution in spin and peak height. Same as Fig. 2, but now incorporating both the predicted shape of the spin parameter distribution and the anticorrelation between spin and peak height. These results are similar to those of Fig. 2; the joint distribution in λ and ν scatters the predictions roughly along the TF relation itself, tightening the TF relation slightly, particularly in bluer bands.

$\Omega_0 = 0.3$, $h = 0.65$, a Salpeter IMF and the joint distribution in λ and ν, as well as chemical evolution. We refer to this particular model as the 'A' model. While this is not necessarily the best-fitting model over our entire parameter space, it does yield remarkable agreement with the data, as shown in Fig. 13, and these model parameters fall nicely in line with current observational constraints. In addition to σ and p, the plots list the predicted normalizations and slopes [given by a and b in equation (1)]. The A model appears to fit the slope, normalization and scatter of the TF relation reasonably well in all bands. The predicted scatter in B, however, remains about 0.2 mag higher than observed.

Several factors may account for the slight overprediction of the B-band scatter. One possibility is that our models overestimate the peak luminosity for a given mass. This might be the case, for example, if supernova feedback played a significant role in removing the gas. It is unclear to what extent the energy they release alters the global properties of spirals. If they serve only to 'puff up' the gas distribution (MacLow & Ferrara 1999), then our model would remain effectively unchanged. If they expel gas from the halo, this could alter our predictions. The inclusion of feedback is known to improve the agreement at the faint end of the B-band LF (Somerville & Primack 1999). Our predictions for the mean TF relation, however, match B-band data down to $V_c = 50\,\mathrm{km\,s^{-1}}$. Strong feedback would not only disrupt this agreement for low V_c, but also alter the predictions at other wavelengths. Some recent observations do indicate a break in the near-IR TF relation at $V_c \sim 90\,\mathrm{km\,s^{-1}}$ (McGaugh et al. 2000), but this is due to extremely gas-rich galaxies, and a single linear relation can be restored by considering total disc mass in place of luminosity. Fine tuning by supernovae of the gas mass available for star formation would be allowed by our model and could tighten the TF scatter in B. Similarly, the assumption of a more realistic density profile, one flatter near the core than our isothermal profile, would result in a slightly lower SFR and thus slightly fainter magnitudes for actively star-forming galaxies near the magnitude peak. The effects of these kinds of modifications, which might tend only to produce small changes in the amount of gas available for star formation, would be largely confined to B, presumably resulting in a slight dimming and tightening of the B-band predictions and bringing them more in line with the observations. It should also be noted that the accuracy of dust corrections can have a significant impact in bluer bands (Avila-Reese & Firmani 2000a).

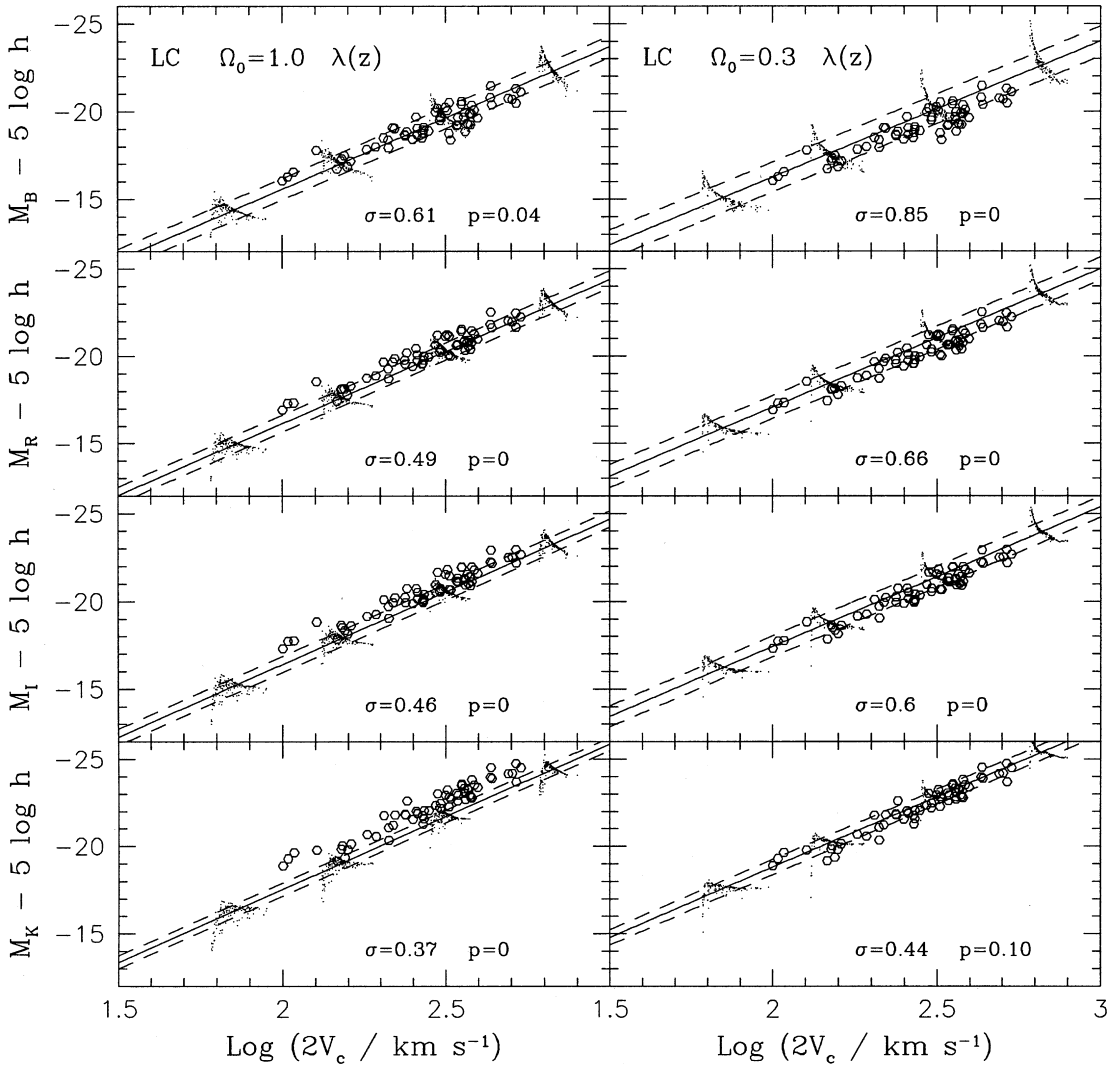

Figure 10. Same as Fig. 3, but now incorporating the joint PDF in λ and ν into the LC results.

Fig. 14 shows the predictions of the A model for the TF relation at $z = 1$, together with six data points from Vogt et al. (1997) for spirals in the range $0.5 < z < 1.0$. These data have been corrected for dust and the *k*-correction has been applied. At $z = 1$ our model predicts larger values of a (i.e. fainter zero-points) and steeper slopes for the TF relation in every band, as compared to $z = 0$. This results in the TF relation becoming about 1 mag brighter at $50\,\mathrm{km\,s^{-1}}$ and about 2 mag brighter at $500\,\mathrm{km\,s^{-1}}$ in the *B* band, but conspires to produce very little change at these scales in the *K* band. Moreover, the scatter in the TF relation in all bands at $z = 1$ is predicted to be roughly the same as that at $z = 0$, though we do not impose any colour selection criterion in the high-redshift case, since it is not as clear what the observational selections are. The similar scatter is due to the fact that, though more galaxies fall on the young side of the magnitude peak for a given mass, many galaxies still form before $z = 1$ and are sufficiently old to trace out the full TF spread down to the oldest, reddest envelope of objects. Though the *B*-band data shown comprise only six points, they have an intrinsic scatter consistent with that of the low-*z* data and are fitted by our model extremely well ($p = 0.36$), though, as in the $z = 0$ case, the predicted scatter is about 0.2 mag too large.

Avila-Reese & Firmani (2000b) investigate TF predictions at comparable redshifts. They also predict a $z = 1$ infrared TF relation with a similar slope and slightly fainter zero-point, but increased star formation rates in their model lead to a shallower *B*-band slope and brighter zero-point at $z = 1$, in contrast to our results. The difference may be due to the fact that their *B*-band predictions rely on luminosity-dependent dust corrections to obtain accurate results at $z = 0$, rather than following naturally from their stellar populations modelling (Avila-Reese & Firmani 2000a). Our predictions seem to match the available data better at high redshift, but further investigation is needed to understand precisely how to construct and interpret data properly at high *z*. Buchalter et al. (in preparation) explore the model predictions at even higher redshifts, and find that the TF scatter in particular can serve as an important diagnostic of the star formation history, and distinguish between models that have similar features at $z = 0$. It should be noted that the points in Fig. 14 correspond to objects that were selected to resemble local disc galaxies. It is not clear to what extent such objects fairly sample the overall galaxy population at high redshift. In particular, other observations seem to suggest that, beyond the local universe, 'normal' galaxies actively form stars primarily in their small cores (see, e.g., Rix et al. 1997; Simard & Pritchet 1998). Linewidth measurements of star-forming galaxies at $z = 1$ and beyond are found to sample effectively only the core dispersion, yielding typical values of

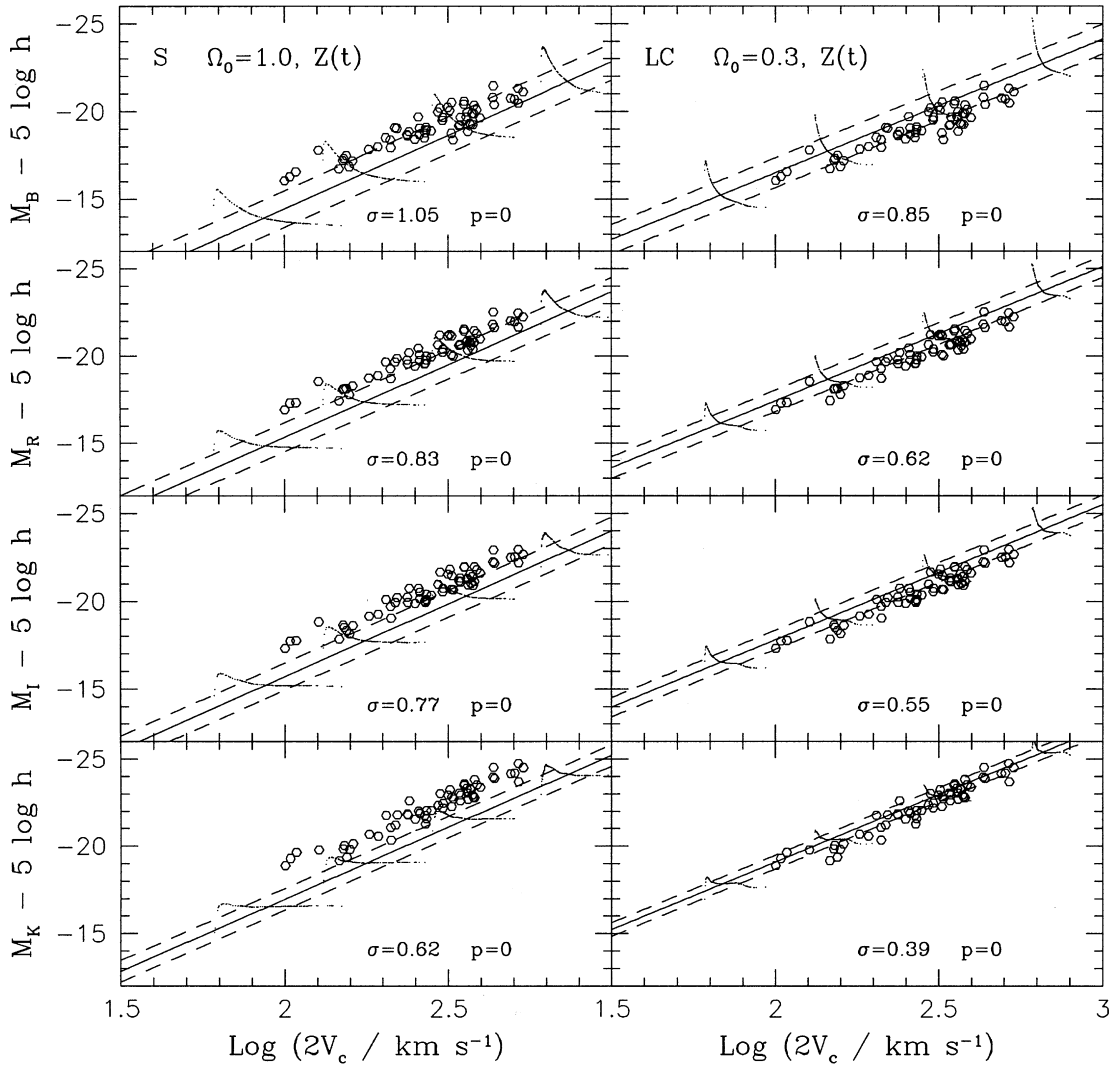

Figure 11. Effect of chemical evolution. TF predictions for an $\Omega_0 = 1$ S distribution (left panels) and an $f = 0.75$ LC distribution with $\Omega_0 = 0.3$ (right panels), both with evolving metallicity. Note the smaller TF scatter as compared to the corresponding results in Figs 2 and 3.

roughly $80\,\mathrm{km\,s^{-1}}$ with a scatter of about 20–$30\,\mathrm{km\,s^{-1}}$ over a range of several magnitudes (Steidel, private communication; Adelberger, private communication). Unless improved measurements can succeed in sampling the disc at larger radii (or at some other means of tracing the potential), a proper TF relation cannot be easily defined.

4.2 The surface brightness–magnitude relation

The TF relation, while important, is but one of many pieces of observational data on disc galaxies. One very interesting test that is often overlooked is that of the surface brightness–magnitude relation. The solid lines in the left- and right-hand panels of Fig. 15 show our A-model prediction for the mean *B*-band surface brightness within the disc scalelength, R_d (see equation 12), as a function of magnitude, for $z = 0$ and $z = 0.4$, respectively; the dashed lines are the 1σ bounds. The dots are the data from Driver & Cross (2000) derived from the 2dF survey, and the open triangles are data from Driver et al. (1999), who used a volume-limited sample derived from the *Hubble Deep Field* (HDF). We have also included the location of the anomalous low surface brightness giant Malin 1 in the $z = 0$ plot. No colour cuts have been imposed. Although the model predictions in the right panel are for $z = 0.4$, the mean redshift for the galaxies in the HDF data set, the brightening of galaxies between $z = 0.1$ and 0.4 will have a minor impact on the outcome of the fit. We also note that the data correspond to effective surface brightness as defined in Driver et al. (1999), and therefore include a bulge component that is absent in our computed central surface brightness for an exponential disc,[10] so we might expect our model to underpredict the normalization.

The first striking feature of the data is that there exists a correlation between absolute magnitude and surface brightness, as first discovered by Binggeli & Cameron (1991) for the Virgo population and later confirmed for the field population by Driver et al. (1999). Gratifyingly enough, our model predicts a similar correlation, which produces a reasonable fit. Ignoring the highest and lowest points in the HDF data, the predicted slopes match well to those observed. The predictions are indeed slightly fainter,

[10] Note that the data points are slightly higher than the Freeman law (Freeman 1970; Driver et al. 1999).

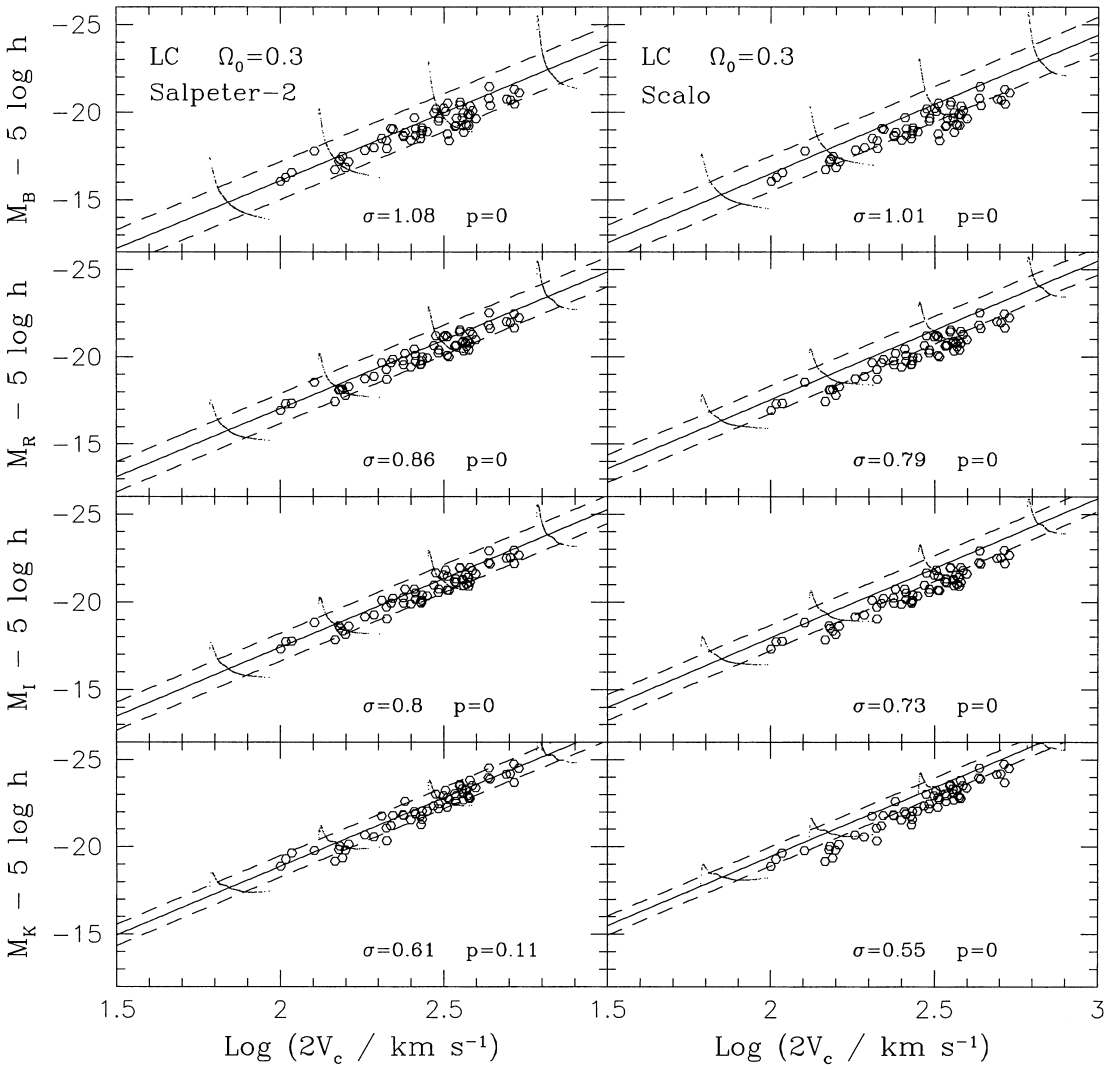

Figure 12. Dependence on the IMF. TF predictions for an $f = 0.75$ LC distribution with $\Omega_0 = 0.3$, assuming a Salpeter IMF with index $\alpha = 0.95$ (left panels) and a Scalo IMF (right panels). These IMFs produce relatively more massive stars than the $\alpha = 1.35$ Salpeter IMF investigated previously, but similar TF predictions to those in the right panels of Fig. 3, since there is little ongoing star formation in these systems at $z = 0$.

possibly due to the reasons detailed above and/or to observational biases against low surface brightness galaxies in the HDF and 2dF surveys, and manifest a scatter only about 15 per cent larger than that *currently* observed. Until more complete surveys can determine the precise scatter of the surface brightness–magnitude relation, it is too early to conclude if our model predicts a scatter that is in fact too large.

As already proposed by Driver & Cross (2000), this relation offers a physical alternative to the 'botanical' Hubble galaxy classification scheme [see fig. 4 in Driver & Cross (2000)], with the *x*-axis determined by the mass and the *y*-axis determined primarily by the angular momentum of the dark halo. Here we confirm that the *x*-axis is indeed determined by the mass, but the *y*-axis is determined both by the spin of the halo (λ) *and* by the redshift of formation (i.e. by the initial conditions). It is also reassuring to find that our model predicts that low surface brightness giants like Malin 1 should be very rare objects (about 4σ fluctuations), which agrees well with the observed paucity of these objects. As was the case for the TF predictions, most other models investigated (with different cosmogonies and so on) grossly failed to fit the data. Unlike the TF predictions, however, the surface brightness predictions do depend sensitively on λ (which fixes the radial scalelength; see also Firmani & Avila-Reese 2000) and thus provide a strong complementary constraint on the models.

4.3 Other considerations

McGaugh & de Blok (1997) examine a host of properties, including mass-to-light ratio, gas fraction, surface brightness, magnitude, scalelength, colour and morphology, for a large sample of spiral galaxies, and find evidence for several strong correlations between various parameters. Our A-model predictions reproduce the sense of these various correlations in almost every case. In particular, we find positive correlations between gas fraction and magnitude, gas fraction and surface brightness, and scalelength and surface brightness, a negative correlation between scalelength and magnitude, and little or no correlation between scalelength and gas fraction. In general, however, the strength of the predicted correlations is significantly weaker than observed by McGaugh & de Blok (1997). The discrepancy probably arises in part from the lower gas fractions predicted by our model, but

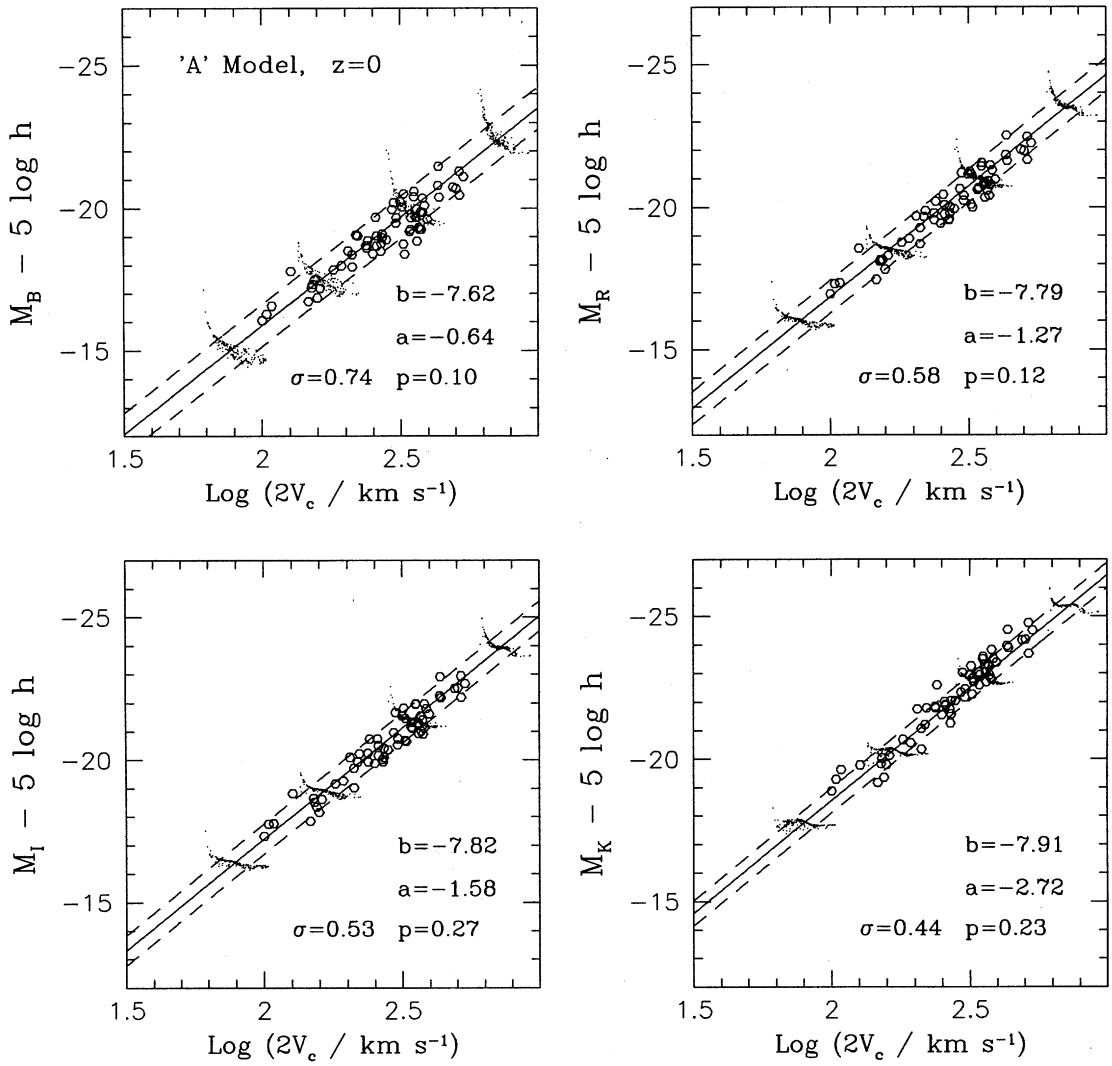

Figure 13. Agreement of the 'A' model. Present-day TF predictions for the 'A' model in *B*, *R*, *I* and *K* for a *COBE*-normalized $f = 0.5$ LC distribution with $\Omega_0 = 0.3$, $h = 0.65$, a Salpeter IMF, including the joint distribution in λ and ν as well as chemical evolution. This model, denoted as the 'A' model, produces excellent agreement in all bands ($p > 0.10$) with roughly the correct amount of scatter ($\sigma \sim 0.4$–0.5).

undoubtedly as well from inconsistencies between the two sample definitions. While we investigate all objects produced by our model, including recently formed starbursting galaxies, high-spin galaxies with low surface brightness and so on, the McGaugh & de Blok (1997) sample was defined on the basis of colour, morphology and other criteria, and is subject to observational selection effects which we have not sought to reproduce. Still, the fact that we obtain the correct sense for the various trends is encouraging, and future work will be aimed at a more valid comparison with such data.

Another obvious test one can apply is the observed luminosity function of disc galaxies. In the context of our model, the LF is given by $\mathrm{d}n/\mathrm{d}M_\lambda = (\mathrm{d}n/\mathrm{d}M)\,\mathrm{d}M/\mathrm{d}M_\lambda$, where $\mathrm{d}n/\mathrm{d}M$ is the number density of objects, per unit mass, obtained from equation (7). An equation for $\mathrm{d}M/\mathrm{d}M_\lambda$ can be derived from the model outputs assuming the mass–magnitude relationship obeys a power law, which is an excellent assumption at these scales, and dust corrections (e.g. Wang & Heckman 1996) can then be applied.

Owing to the uncertainty in the precise normalization of the M–V_c relation (and thus the derived mass–magnitude relationship) in our singular isothermal model, however, the precise normalization of the LF cannot be determined. In other words, ascribing a different V_c to a fixed mass will alter the predicted magnitude, but not the PS prediction for number density of haloes with this mass. Adding to this the well-known shortcomings and limitations of the PS formalism (e.g. Tormen 1998; Somerville et al. 2000; Gardner 2000), particularly in accurately predicting number densities of sub-$L*$ haloes, and the uncertainties in the present LF data, we do not investigate LF predictions in the context of our simplified model.

Interestingly, the uncertainty in the normalization of the M–V_c relation does not seriously impact the other relations investigated here. For the TF and surface brightness–magnitude relations, both well approximated by power laws over these scales, this uncertainty enters into both axes, offsetting so as to leave little or no net effect. Ascribing a higher V_c to a fixed mass will simply result in a correspondingly higher luminosity, as per equation (2), simply shifting our predictions along the TF relation. We further investigated this point by comparing our A-model results to those

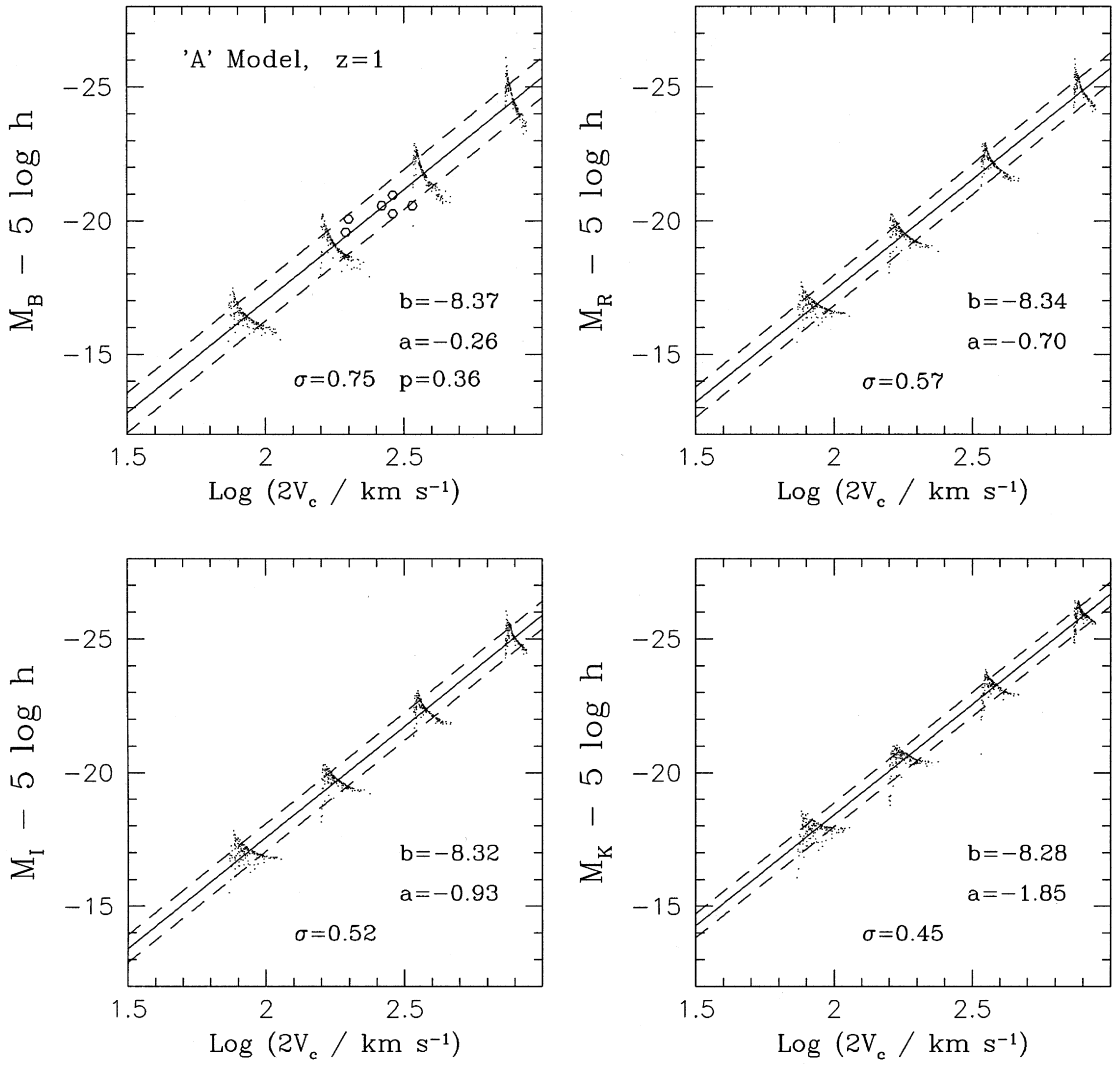

Figure 14. High-redshift predictions. TF prediction of the 'A' model for $z = 1$, along with six *B*-band data points from Vogt et al. (1997) for spirals in the range $0.5 < z < 1$. The $z = 1$ predictions have steeper slopes (given by *b*) and lower zero-points (given by *a*) than the counterpart $z = 0$ predictions, resulting in a brighter *B*-band TF relation, but roughly a roughly similar relation in *K*.

obtained using the M–V_c relation of Wang & Steinhardt (1998) for a constant-density halo, with varying values for the constant of proportionality in this relation. Despite the slightly different redshift dependences and the variation of a factor of 2 in the circular velocity ascribed to a given mass, we nonetheless found the resulting A models in the different cases to have exactly the same parameter values, with the exception of h, which ranged from 0.65 to 0.70. Similarly, for the suite of models investigated in Figs 2 to 12 and for the A-model surface brightness–magnitude relation, the impact of this variation was minimal, typically smaller than the statistical uncertainty of the predictions. Thus, unlike the LF, which relies on precise number density predictions, our conclusions with respect to the scaling relations investigated are fairly robust to the uncertainty in the M–V_c relation. Still, one should be careful not to overinterpret the precise absolute values we obtain here, such as for the TF normalizations, the predicted remaining gas fraction, or the boundaries of the A-model formation redshift range; greater confidence should be placed in relative differences between models. Ultimately, features such as universal profiles and adiabatic contraction will be needed to ascertain precise absolute values for our predictions.

5 CONCLUSIONS

We have constructed a largely analytic disc-galaxy model, built on that of HJ99, which incorporates such features as the halo formation redshift distribution, the joint distribution in spin and peak height, the dependence on the cosmological model and star formation with chemical evolution. The model contains fewer free parameters than previous SAMs – the main dependences are on cosmological parameters, and these are ultimately chosen to be consistent with current estimates – and yet yields remarkable agreement with the observed TF relation and other disc-galaxy properties. Varying these inputs and exploring the model's predictions over a range of wavebands, we find that both parent halo features and stellar evolution play a role in defining the TF relation and other disc-galaxy properties; the former fixes the overall relation and spread, while the latter fine tunes these to

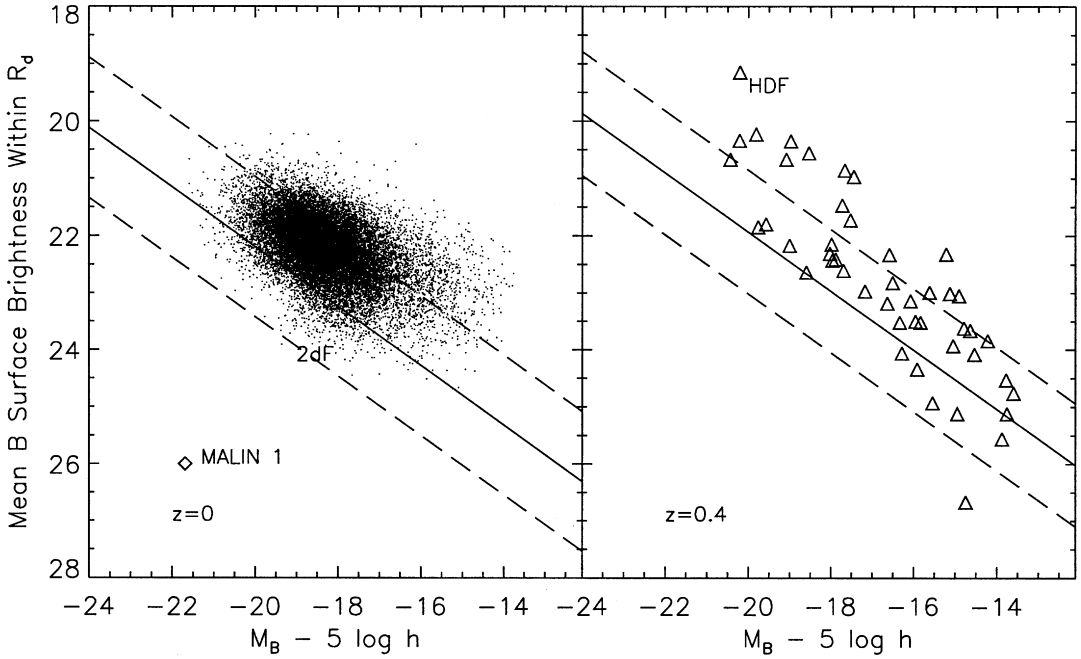

Figure 15. The surface brightness–magnitude relation. 'A'-model predictions for the mean *B*-band surface brightness as a function of magnitude (solid line) at $z = 0.4$, which corresponds to the mean redshift of the HDF data points (open triangles; taken from Driver et al. 1999). The dots are the data from Driver & Cross (2000), derived from the 2dF survey. The dashed lines show the 1σ error in the prediction. We have also included the location of the anomalous low surface brightness giant Malin 1.

observed levels. Our investigation has yielded a number of specific results:

(i) We confirm that the TF relation broadly arises as a signature of gravitational instability acting upon cosmological initial conditions and that the spread in halo formation redshifts is the primary source of scatter in the TF relation (EL96; Firmani & Avila-Reese 2000). In agreement with previous studies, we predict a TF relation that generally broadens with decreasing V_c and exhibits increasingly large scatter towards bluer wavebands (HJ99; Somerville & Primack 1999; van den Bosch 2000). For the local *K*-band TF relation at all but the largest and youngest masses, the TF scatter couples only to V_c; in bluer bands the scatter couples to both axes, as younger systems have both lower V_c and higher *B*-band luminosity.

(ii) We find that disc galaxies in $\Omega_0 = 1$ models are generally too faint to match the observed TF relation, but, contrary to the claim of van den Bosch (2000), this result does not depend on the inclusion of adiabatic disc contraction, universal halo profiles (Navarro, Frenk & White 1997), or the precise definition of V_c. We find that successful models tend to favour low values of $\Omega_0 h \sim 0.2$ and in particular $\Omega_0 \sim 0.3$ and $h \sim 0.65$ (assuming *COBE* normalization), in agreement with previous work (Somerville & Primack 1999; van den Bosch 2000; Firmani & Avila-Reese 2000).[11]

[11] Recent preliminary results from the BOOMERANG (Lange et al. 2000) and MAXIMA (Lee et al. 1999) experiments point to larger values of $\Omega_b h^2$ (Enqvist, Kurki-Suonio & Valiviita 2000; Hanany et al. 2000; Jaffe et al. 2000). A higher baryon fraction would brighten the TF predictions, but this could be counteracted by a slightly higher value of h (or by changing other input parameters so as still to remain within current constraints), so as to yield a similarly well-fitting model. Many of the conclusions presented here are robust with respect to the precise values of these various parameters.

(iii) The inclusion of the spin parameter distribution, with an anticorrelation with peak height, tends to act along the TF axis itself, and can therefore slightly reduce the TF scatter in some models, but does not otherwise have a major impact on the TF relation. Thus, uncertainties in obtaining accurate λ distributions, such as non-linear effects, proper calculation of binding energies and so on, are probably unimportant. The spin distribution is important, however, in determining disc scalelengths and surface brightnesses, which can provide independent tests of the model. These conclusions are roughly in agreement with the results of more complicated modelling by Avila-Reese & Firmani (2000a), although their models did not account for the possible correlation between peak height and spin, thus potentially overestimating the impact of the spin distribution on the TF scatter.

(iv) The incorporation of chemical evolution leads to older (younger) populations which are brighter (fainter), leading to a reduction of TF scatter of about 0.1 mag in all wavebands.

(v) Many models can be found to yield reasonable agreement with the data in one or two bands, but not in others. Typically, *I* and *K* data are the easiest to fit, since these wavelengths are largely detached from the star formation history. Imposing multiwavelength constraints, however, provides a strong discriminator among models.

(vi) Models that yield the best agreement with TF data across *all* wavelengths have cosmological parameter values in good agreement with current estimates and require that the majority of discs form in the range $0.4 < z < 2.0$, with little subsequent accretion, as suggested by Peebles (2000). In particular, the reasonable agreement in *B* seems to rule out very late collapse. The $f = 0.5$ LC distribution appears to represent a suitable choice for the range of halo formation redshifts. Note that this agreement is obtained with a spread in z_f of $\Delta z_f/(1 + z_f) \sim 0.5$, considerably larger than that suggested by the results of Eisenstein & Loeb

(1996) and van den Bosch (2000), demonstrating the impact of regulating effects from stellar evolution and metal enrichment.

Though, as mentioned above, care should be taken not to overinterpret the precise boundaries of the halo formation epoch, our exploration of the parameter space indicates that, assuming passive star formation according to the empirical Schmidt law, it is difficult to escape the conclusion that discs must have formed in a limited range of redshifts that does not extend much past $z \sim 3$. Regardless of the adopted M–V_c relation, S-distribution models that form appreciable numbers of galaxies beyond $z \sim 3$ cannot be reconciled with local TF data for reasonable choices of cosmogony. Agreement may be possible if one abandons the picture of a monolithic disc passively forming stars at a monotonically decreasing rate from formation to the present day, for example if compact discs form at very high redshift and acquire higher luminosities at later epochs via merging and late infall of fresh gas. Such a scenario is not in the scope of the present model and could not be ruled out here, but other work suggests that obtaining the correct TF scatter would be difficult in such a scenario (EL96; van den Bosch 2000).

(vii) Models fitting the TF relation at $z = 0$ also appear to obtain the correct, steeper B-band TF relation at $z = 1$, and predict a near-IR $z = 1$ TF relation that is essentially identical to the local one at the scales investigated.

(viii) Successful models also roughly match the observed surface brightness distribution of spirals and reproduce the sense of observed trends between other sets of disc properties.

(ix) Our simple model, which contains fewer free parameters than typical SAMs, goes a long way in obtaining correct disc-galaxy scaling relations, without including many of the higher-order details in other galaxy formation recipes. This may provide important clues in constructing more sophisticated and realistic models. In general, this success argues that there is probably little room for stochasticity arising from other complicating effects, such as mergers or supernova feedback. Spiral galaxies appear to behave like island universes (MacLow & Ferrara 1999; Peebles 2000). Small variations to the disc baryon content from such mechanisms could still be tolerated, though their effects would be largely confined to the B band. Modelling these weaker effects might serve to improve the model's predictions for the B-band TF relation.

There are several features common to many SAMs that have not been incorporated into our framework, as these do not appear to impact strongly on the properties investigated here. For example, we adopt an isothermal profile, rather than the universal form of Navarro et al. (1997). While observations, as well as some simulations, indicate that real haloes do resemble truncated isothermal spheres, rather than universal profiles (Dubinski & Carlberg 1991; Spergel & Hernquist 1992; Sellwood 1999), our model is clearly too steep in the core. For our purposes, however, changes to the profile of a halo with a fixed mass are only relevant inasmuch as they alter the local gas surface density and thus the SFR. This is similar to the effect of changing the spin parameter, and we have seen that our model changes relatively little over the broad range investigated in λ and thus Σ (HJ99). Jimenez et al. (1997) developed a similar disc-galaxy model, but explicitly incorporating the universal profile, and found little difference from the results of HJ99. Firmani & Avila-Reese (2000) also find that predictions for global disc-galaxy properties are nearly the same for models with and without a shallow core, suggesting that flatter core profiles are not a crucial ingredient to the model. The excess core gas resulting from the assumption of an isothermal profile might, however, have the effect of making younger galaxies too bright in B. As discussed above, this might partially account for the slightly poorer TF fit and larger predicted scatter in B.

While the assumption of monolithic disc collapse cannot be strictly accurate, accounting for adiabatic disc contraction also does not appear essential to predicting these disc properties. This would have the main effect of altering the rotation velocities predicted for a given mass halo, but we have already seen that the predictions investigated here are fairly robust with respect to such changes. Moreover, adiabatic contraction tends to make spirals more dark matter dominated at the core, whereas observations indicate that they are more baryon dominated (Sellwood 1999). Similarly, the inclusion of a stability threshold criterion for star formation does not appear essential to our results, and some authors have argued against the importance of such a threshold (Ferguson et al. 1998). More sophisticated and realistic models must of course include realistic profiles, adiabatic contraction, a star formation threshold and other features, but our results suggest that they may not play a vital role in fixing the TF relation and other properties.

Another key assumption in this model is that the specific angular momentum of the baryons is the same as that of the dark matter. This is a common assumption of analytic calculations (e.g. Fall & Efstathiou 1980; Mo et al. 1998). Recent observations indicate that this assumption may be well justified. For example, Burkert (2000) concludes that observed low-mass galaxies seem to indicate no loss of angular momentum by the visible baryonic disc. Still, it has been argued on the basis of hydrodynamic simulations that this is not the case; cooling of gas leads to substructure which can couple with the halo, leading to loss of a sizeable fraction of the baryon angular momentum (e.g. Navarro & Benz 1991; Weil, Eke & Efstathiou 1998; Navarro & Steinmetz 2000). The predictions of our model would thus be altered significantly, with much smaller discs, higher early star formation rates and different colours. Therefore we need to assume that such angular momentum loss does not occur in practice. It is fair to say that the question of how (or indeed if) baryon angular momentum is conserved is open at present, although there are plenty of ideas for how the coupling can be prevented. These include gas ejection from sub-units by supernovae (Efstathiou 2000), suppression of gas cooling until the halo is established with a smooth profile (Weil et al. 1998), prevention of formation of small haloes by a cut-off in the power spectrum (Kamionkowski & Liddle 2000), or changing the nature of the dark matter (Spergel & Steinhardt 1999).

A generic problem is the possibility that our model either overpredicts or underpredicts the amount of gas that is converted into disc stars, as a result of effects such as supernova feedback, the presence of hot X-ray gas, or enhanced star formation from late infall. Though we have assumed essentially featureless (in space and time) star formation, the addition or removal of large amounts of gas via such stochastic mechanisms would increase the scatter in the TF relation and shatter the agreement obtained here. To the extent that such processes result in smaller fluctuations to the amount of gas available for star formation, their effects would be confined primarily to B, where our models are indeed weakest. We point out that the Schmidt law implicitly assumes supernova feedback, which can redistribute gas within the disc and serves to delay star formation. It is only inflows and outflows that are not accounted for in our model, and detailed multiphase ISM

simulations seem to indicate that these are negligible and that spirals may be well approximated as 'island universes'. Note also that we may be implicitly assuming some influence of supernova (or other) feedback in keeping the specific angular momentum of the baryons equal to that of the halo (Weil et al. 1998). Mergers probably play only a very limited role. It is well known that classic spirals could not maintain their thin-disc structure in the case of extreme merging. EL96 found that excluding objects that had merged with a mass >20 per cent (as opposed to 50 per cent) of the parent halo reduced the predicted *I*-band scatter by only 20 per cent, suggesting that accretion does not play a major role, or possibly induces scatter along the near-infrared TF relation. Either way, this would imply that the TF relation at higher redshift looks similar to that at $z = 0$, and this is precisely what we find when comparing the $z = 0$ and $z = 1$ TF relations in *I* and *K*. Avila-Reese & Firmani (2000a) also concluded that merging, non-stationary star formation and feedback are effectively only second-order processes with respect to the determination of the properties investigated here. Future work will be aimed at quantitatively assessing the precise impact of these various other mechanisms, as well as obtaining predictions for the high-redshift universe (Buchalter et al., in preparation). While our model is a long way from providing a complete picture of galactosynthesis, our results suggest that future models addressing spiral properties must invariably incorporate detailed star formation, as well as initial conditions, and that features such as exponential discs, little or weak substructure, Schmidt-law star formation and little gas inflow or outflow should be generic predictions of more sophisticated modelling.

ACKNOWLEDGMENTS

We wish to acknowledge the collaboration of A. F. Heavens, whose numerous contributions have greatly enhanced this work. We are indebted to L. Wang for helpful discussions and for providing numerical results pertinent to our cosmological models. We also thank the anonymous referee for valuable and insightful feedback. This work was supported by grants NSF-AST-0096023, NSF-AST-9900866, NSF-AST-9618537, NASA NAG5-8506 and DoE DE-FG03-92-ER40701 and by a PPARC Advanced Fellowship.

REFERENCES

Avila-Reese V., Firmani C., 2000a, Rev. Mex. Astron. Astrophys., 36, 23
Avila-Reese V., Firmani C., 2000b, in Lee W., Torres-Peimbert S., eds, The Seventh Texas–Mexico Conference on Astrophysics: Flows, Blows & Glows. Rev Mex AA (Serie de Conferencias), in press
Avila-Reese V., Firmani C., Hernandez X., 1998, ApJ, 505, 37
Bardeen J. M., Bond J. R., Kaiser N., Szalay A. S., 1986, ApJ, 304, 15
Binggeli B., Cameron L. M., 1991, A&A, 252, 27
Bunn E. F., White M., 1997, ApJ, 480, 6
Burkert A., 2000, ApJL, submitted (astro-ph/0007047)
Catelan P., Theuns T., 1996, MNRAS, 282, 436
Dalcanton J. J., Spergel D. N., Summers F. J., 1997, ApJ, 482, 659
Driver S. P., Cross N., 2000, in Kraan, Korteweg, Henning, Andernach, eds, Mapping the Hidden Universe (astro-ph/0004201)
Driver S. P. et al., 1999, ApJ, 526, L69
Dubinski J., Carlberg R. G., 1991, ApJ, 378, 496
Efstathiou G., 2000, MNRAS, 317, 697
Eisenstein D. J., Loeb A., 1996, ApJ, 459, 432 (EL96)
Enqvist K., Kurki-Suonio H., Valiviita J., 2000, Phys. Rev. D, 62, 103003
Fall S. M., Efstathiou G., 1980, MNRAS, 193, 189
Ferguson A. M. N. et al., 1998, ApJ, 506, L19
Firmani C., Avila-Reese V., 1998, in Observational Cosmology: The Development of Galaxy Systems, ASP Conf. Ser. Vol. 176. Astron. Soc. Pac., San Francisco, p. 406
Firmani C., Avila-Reese V., 2000, MNRAS, 315, 457
Folkes S. R. et al., 1999, MNRAS, 308, 459
Freeman K. C., 1970, ApJ, 160, 811
Gardner J. P., 2000, astro-ph/0006342
Glazebrook K., Ellis R., Santiago B., Griffiths R., 1995, MNRAS, 275, 169
Hanany S. et al., 2000, ApJL, 545, 5
Heavens A. F., Jimenez R., 1999, MNRAS, 305, 770 (HJ99)
Heavens A. F., Peacock J., 1988, MNRAS, 232, 339
Jaffe A. H. et al., 2000, PRL, submitted (astro-ph/0007333)
Jimenez R., Heavens A. F., Hawkins M. R. S., Padoan P., 1997, MNRAS, 292, L5
Jimenez R., Padoan P., Matteucci F., Heavens A. F., 1998, MNRAS, 299, 123
Jimenez R., Padoan P., Dunlop J. S., Bowen D. V., Juvela M., Matteucci F., 2000, MNRAS, ApJ, 532, 152
Kamionkowski M., Buchalter A., 2000, astro-ph/0001045
Kamionkowski M., Liddle A. R., 2000, Phys. Rev. Lett., 84, 4525
Kennicutt R., 1998, ApJ, 498, 541
Lacey C., Cole S., 1993, MNRAS, 262, 627
Lacey C., Cole S., 1994, MNRAS, 271, 676
Lange A. E. et al., 2000, Phys. Rev. D, submitted (astro-ph/0005004)
Lee A. T., 1999, in Maiani L., Melchiorri F., Vittorio N., Proc. EC-TMR Conf. Vol. 476. American Institute of Physics, New York, p. 224
Lemson G., Kauffmann G., 1999, MNRAS, 302, 111
McGaugh S. S., de Blok W. J. G., 1997, ApJ, 481, 689
McGaugh S. S., Schombert J. M., Bothun G. D., de Blok W. J. G., 2000, ApJL, 533, 99
MacLow M.-M., Ferrara A., 1999, ApJ, 513, 142
Mo H. J., Mao S., 2000, 318, 163
Mo H. J., Mao S., White S. D. M., 1998, MNRAS, 295, 319
Navarro J. F., Benz W., 1991, ApJ, 380, 320
Navarro J. F., Steinmetz M., 2000, ApJ, 538, 477
Navarro J. F., Frenk C. S., White S. D. M., 1997, ApJ, 490, 493
Pagel B. E. J., 1997, Nucleosynthesis and Chemical Evolution of Galaxies. Cambridge Univ. Press, Cambridge
Peacock J. A., Dodds S. J., 1994, MNRAS, 267, 1020
Peebles P. J. E., 2000, in Mazure A., Le Fevre O., Le Brun V., eds, ASP Conf. Ser. Vol. 200, Clustering at High Redshift. Astron. Soc. Pac., San Francisco, p. 377
Percival W. J., Miller L., Peacock J. A., 2000, MNRAS, 318, 273
Pettini M., Ellison S. L., Steidel C. C., Bowen D. V., 1999, ApJ, 510, 576
Rix H.-W., Guhathakurta P., Colless M., Ing K., 1997, MNRAS, 285, 779
Sasaki S., 1994, PASJ, 46, 427
Scalo J., 1986, Fundam. Cosmic Phys., 11, 1
Sellwood J. A., 1999, in Merritt D. R., Valluri M., Sellwood J. A., eds, ASP Conf. Ser. Vol. 182, Galaxy Dynamics. Astron. Soc. Pac., San Francisco
Silk J., 1997, ApJ, 481, 703
Simard L., Pritchet C. J., 1998, ApJ, 505, 96
Somerville R. S., Primack J. R., 1999, MNRAS, 310, 1087
Somerville R. S., Lemson G., Kolatt T. S., Dekel A., 2000, MNRAS, 316, 479
Spergel D. N., Hernquist L., 1992, ApJ, 397, L75
Spergel D. N., Steinhardt P. J., 1999, Phys. Rev. Lett., 84, 3760
Sprayberry D., Bernstein G. M., Impey C. D., Bothun G. D., 1995, ApJ, 438, 72
Tormen G., 1998, MNRAS, 297, 648
Tully R. B., Pierce M. J., Huang J.-S., Saunders W., Verheijen M. A. W., Witchalls P. L., 1998, AJ, 115, 2264
Tytler D., Burles S., Lu L., Fan X.-M., Wolfe A., Savage B. D., 1999, ApJ, AJ, 117, 63
Ueda H., Shimasaku K., Suginohara T., Suto Y., 1994, PASJ, 46, 319
van den Bosch F. C., 2000, ApJ, 530, 177
Viana P. T. P., Liddle A. R., 1996, MNRAS, 281, 323

Vogt N. P. et al., 1997, ApJ, 479, L121
Wang B., Heckman T., 1996, ApJ, 457, 645
Wang L., Steinhardt P. J., 1998, ApJ, 508, 483
Weil M. L., Eke V. R., Efstathiou G., 1998, MNRAS, 300, 773
Willick J. A., Courteau S., Faber S. M., Burstein D., Dekel A., Kolatt T., 1995, ApJ, 446, 12
Willick J. A., Courteau S., Faber S. M., Burstein D., Dekel A., 1996, ApJ, 457, 460
Willick J. A., Courteau S., Faber S. M., Burstein D., Dekel A., Strauss M. A., 1997, ApJS, 109, 333
Zucca E. et al., 1997, A&A, 326, 477
Zwaan M. A. et al., 1995, MNRAS, 273, 35

APPENDIX A: LUMINOSITIES AND ANALYTIC FITS

The luminosity of an arbitrary stellar population can be computed analytically as follows. Simple stellar populations (SSPs) are the building blocks of any arbitrarily complicated population since the latter can be computed as a sum of SSPs, once the star formation rate is provided. In other words, the luminosity of a stellar population of age t_0 (since the beginning of star formation), in waveband λ, can be written as:

$$L_\lambda(t_0) = \int_0^{t_0}\int_{Z_\mathrm{i}}^{Z_\mathrm{f}} L_{\mathrm{SSP},\lambda}(Z, t_0 - t)\,\mathrm{d}Z\,\mathrm{d}t, \tag{A1}$$

where the luminosity of the SSP is

$$L_{\mathrm{SSP},\lambda}(Z, t_0 - t) = \int_{M_\mathrm{min}}^{M_\mathrm{max}} \mathrm{SFR}(Z, M, t) l_\lambda(Z, M, t_0 - t)\frac{\mathrm{d}N}{\mathrm{d}M}\,\mathrm{d}M \tag{A2}$$

and $l_\lambda(Z, M, t_0 - t)$ is the luminosity of a star of mass M, metallicity Z and age $t_0 - t$, Z_i and Z_f are the initial and final metallicities, $\mathrm{d}N/\mathrm{d}M$ represents the IMF, M_min and M_max are the smallest and largest stellar mass in the population, and $\mathrm{SFR}(Z, M, t)$ is the star formation rate at the time t when the SSP is formed.

The magnitudes for an SSP (normalized to $1\,\mathrm{M}_\odot$) as a function of age and metallicity, for a given photometric band *UBVRIJK*, are approximated to within 4 per cent by

$$M_\lambda = -2.5 \times \sum_{i=0}^{4}\sum_{j=0}^{4} X^i C_\lambda(i+1, j+1) Y^j, \tag{A3}$$

where

$$X = 5.76 + 3.18\log\tau + 1.26\log^2\tau + 2.64\log^3\tau + 1.81\log^4\tau + 0.38\log^5\tau, \tag{A4}$$

$$Y = 2.0 + 2.059\log\zeta + 1.041\log^2\zeta + 0.172\log^3\zeta - 0.042\log^4\zeta, \tag{A5}$$

$$\tau = \frac{t}{\mathrm{Gyr}}, \qquad \zeta = \frac{Z}{Z_\odot}, \tag{A6}$$

and we have assumed a standard Salpeter IMF. Luminosities are obtained simply from

$$L_\lambda = 10^{-0.4(M_{\odot\lambda} - M_\lambda)},$$

where

$$M_{\odot\lambda} = \{5.61, 5.48, 4.83, 4.34, 4.13, 3.72, 3.36, 3.30, 3.28\} \qquad \text{for} \qquad \{U, B, V, R, I, J, H, K, L\}.$$

The i and j values appear as exponents of X and Y, respectively, and as indices defining elements of the C_λ matrices, given by

$$C_U = \begin{pmatrix} -4.738\times10^{-1} & 4.029\times10^{-1} & -3.690\times10^{-1} & 1.175\times10^{-1} & -1.253\times10^{-2} \\ -2.096\times10^{-1} & -1.743\times10^{-1} & 1.268\times10^{-1} & -2.526\times10^{-2} & 8.922\times10^{-4} \\ -1.939\times10^{-2} & 1.401\times10^{-2} & -9.628\times10^{-3} & -1.754\times10^{-3} & 7.237\times10^{-4} \\ 2.671\times10^{-3} & -4.271\times10^{-4} & 2.470\times10^{-4} & 2.963\times10^{-4} & -7.334\times10^{-5} \\ -7.468\times10^{-5} & 6.676\times10^{-7} & 1.482\times10^{-6} & -9.594\times10^{-6} & 2.055\times10^{-6} \end{pmatrix}, \tag{A7}$$

$$C_B = \begin{pmatrix} -8.321\times10^{-1} & 5.972\times10^{-1} & -4.818\times10^{-1} & 1.356\times10^{-1} & -1.271\times10^{-2} \\ -1.223\times10^{-1} & -2.523\times10^{-1} & 2.117\times10^{-1} & -5.309\times10^{-2} & 3.716\times10^{-3} \\ -2.632\times10^{-2} & 2.468\times10^{-2} & -2.462\times10^{-2} & 4.163\times10^{-3} & 5.054\times10^{-5} \\ 2.835\times10^{-3} & -7.906\times10^{-4} & 9.653\times10^{-4} & -1.164\times10^{-5} & -3.800\times10^{-5} \\ -7.416\times10^{-5} & 1.120\times10^{-6} & -6.707\times10^{-6} & -5.615\times10^{-6} & 1.611\times10^{-6} \end{pmatrix}, \tag{A8}$$

$$C_V = \begin{pmatrix} -9.348\times10^{-1} & 7.376\times10^{-1} & -5.170\times10^{-1} & 1.182\times10^{-1} & -8.023\times10^{-3} \\ -9.521\times10^{-2} & -3.476\times10^{-1} & 2.379\times10^{-1} & -4.485\times10^{-2} & 1.303\times10^{-3} \\ -2.437\times10^{-2} & 4.413\times10^{-2} & -2.802\times10^{-2} & 2.202\times10^{-3} & 5.271\times10^{-4} \\ 2.625\times10^{-3} & -2.063\times10^{-3} & 9.257\times10^{-4} & 2.378\times10^{-4} & -8.471\times10^{-5} \\ -6.994\times10^{-5} & 2.842\times10^{-5} & 7.436\times10^{-7} & -1.424\times10^{-5} & 3.050\times10^{-6} \end{pmatrix}, \tag{A9}$$

$$C_R = \begin{pmatrix} -9.755\times10^{-1} & 8.121\times10^{-1} & -4.535\times10^{-1} & 5.553\times10^{-2} & 3.313\times10^{-3} \\ -7.346\times10^{-2} & -4.000\times10^{-1} & 1.983\times10^{-1} & -6.018\times10^{-3} & -5.621\times10^{-3} \\ -2.368\times10^{-2} & 5.415\times10^{-2} & -1.968\times10^{-2} & -5.209\times10^{-3} & 1.811\times10^{-3} \\ 2.502\times10^{-3} & -2.667\times10^{-3} & 1.376\times10^{-4} & 8.392\times10^{-4} & -1.845\times10^{-4} \\ -6.690\times10^{-5} & 4.003\times10^{-5} & 2.413\times10^{-5} & -3.043\times10^{-5} & 5.650\times10^{-6} \end{pmatrix}, \tag{A10}$$

$$C_I = \begin{pmatrix} -1.027\times10^{0} & 8.951\times10^{-1} & -3.759\times10^{-1} & -1.908\times10^{-2} & 1.690\times10^{-2} \\ -4.672\times10^{-2} & -4.514\times10^{-1} & 1.411\times10^{-1} & 4.385\times10^{-2} & -1.440\times10^{-2} \\ -2.379\times10^{-2} & 6.399\times10^{-2} & -8.885\times10^{-3} & -1.425\times10^{-2} & 3.380\times10^{-3} \\ 2.414\times10^{-3} & -3.267\times10^{-3} & -7.741\times10^{-4} & 1.532\times10^{-3} & -3.012\times10^{-4} \\ -6.417\times10^{-5} & 5.166\times10^{-5} & 4.964\times10^{-5} & -4.843\times10^{-5} & 8.607\times10^{-6} \end{pmatrix}, \tag{A11}$$

$$C_J = \begin{pmatrix} -1.106\times10^{0} & 1.043\times10^{0} & -1.932\times10^{-1} & -1.715\times10^{-1} & 4.364\times10^{-2} \\ 1.122\times10^{-2} & -5.240\times10^{-1} & -6.001\times10^{-3} & 1.510\times10^{-1} & -3.228\times10^{-2} \\ -2.757\times10^{-2} & 7.613\times10^{-2} & 1.935\times10^{-2} & -3.358\times10^{-2} & 6.540\times10^{-3} \\ 2.502\times10^{-3} & -3.923\times10^{-3} & -2.956\times10^{-3} & 2.944\times10^{-3} & -5.274\times10^{-4} \\ -6.439\times10^{-5} & 6.234\times10^{-5} & 1.066\times10^{-4} & -8.371\times10^{-5} & 1.417\times10^{-5} \end{pmatrix}, \tag{A12}$$

$$C_K = \begin{pmatrix} -1.132\times10^{0} & 1.296\times10^{0} & -1.795\times10^{-1} & -2.391\times10^{-1} & 5.794\times10^{-2} \\ 6.838\times10^{-2} & -6.627\times10^{-1} & -5.987\times10^{-2} & 2.115\times10^{-1} & -4.319\times10^{-2} \\ -3.194\times10^{-2} & 1.009\times10^{-1} & 3.092\times10^{-2} & -4.459\times10^{-2} & 8.454\times10^{-3} \\ 2.649\times10^{-3} & -5.499\times10^{-3} & -3.923\times10^{-3} & 3.748\times10^{-3} & -6.625\times10^{-4} \\ -6.607\times10^{-5} & 9.556\times10^{-5} & 1.332\times10^{-4} & -1.038\times10^{-4} & 1.746\times10^{-5} \end{pmatrix}. \tag{A13}$$

This paper has been typeset from a TEX/LATEX file prepared by the author.